

~~CONFIDENTIAL~~

Copy 287

RM A54L10

NACA RM A54L10



RESEARCH MEMORANDUM

A COMPARATIVE ANALYSIS OF THE PERFORMANCE OF
LONG-RANGE HYPERVELOCITY VEHICLES

By Alfred J. Eggers, Jr., H. Julian Allen,
and Stanford E. Neice

Ames Aeronautical Laboratory
Moffett Field, Calif.

Decl. TPA63, 1-5-62 WRC.

Maurin F. Tommes

This material contains information affecting the National Defense of the United States within the meaning of the espionage laws, the transmission or the revelation of which in any manner to an unauthorized person is prohibited by law.

**NATIONAL ADVISORY COMMITTEE
FOR AERONAUTICS**

WASHINGTON

March 24, 1955

~~CONFIDENTIAL~~

TABLE OF CONTENTS

	Page
SUMMARY	1
INTRODUCTION	2
ANALYSIS	3
General Considerations	3
Powered Flight and the Breguet Range Equation	3
Motion in Unpowered Flight	6
Ballistic trajectory	6
Skip trajectory	8
Glide trajectory	12
Heating in Unpowered Flight	14
General considerations	14
Ballistic vehicle	18
Skip vehicle	19
Glide vehicle	22
DISCUSSION	26
Performance of Hypervelocity Vehicles	26
Motion	27
Aerodynamic heating	27
Comparison of Hypervelocity Vehicles With the Supersonic Airplane	30
CONCLUDING REMARKS AND SOME DESIGN CONSIDERATIONS FOR GLIDE VEHICLES	31
APPENDIX A - NOTATION	34
Subscripts	36
APPENDIX B - SIMPLIFYING ASSUMPTIONS IN THE ANALYSIS OF THE GLIDE TRAJECTORY	37
APPENDIX C - THE RELATION BETWEEN $C_F'S/C_{DA}$ and $(L/D)_{max}$ FOR CONICAL MISSILES	39
APPENDIX D - COMPUTATION OF HEATING ASSOCIATED WITH ROCKET VEHICLES	44
Radiation of Heat From Glide Vehicles	44
Radiative and Convective Heat Transfer Associated With Skip Vehicle	45
APPENDIX E - DETERMINATION OF THE RATIO OF $(L/D)_{max}$ FOR A FLAT PLATE TO $(L/D)_{max}$ FOR A CONE	49
REFERENCES	52
FIGURES	55



NATIONAL ADVISORY COMMITTEE FOR AERONAUTICS

RESEARCH MEMORANDUM

A COMPARATIVE ANALYSIS OF THE PERFORMANCE OF

LONG-RANGE HYPERVELOCITY VEHICLES

By Alfred J. Eggers, Jr., H. Julian Allen,
and Stanford E. Neice

SUMMARY

Long-range hypervelocity vehicles are studied in terms of their motion in powered flight, and their motion and aerodynamic heating in unpowered flight. Powered flight is analyzed for an idealized propulsion system which rather closely approaches present-day rocket motors. Unpowered flight is characterized by a return to earth along a ballistic, skip, or glide trajectory. Only those trajectories are treated which yield the maximum range for a given velocity at the end of powered flight. Aerodynamic heating is treated in a manner similar to that employed previously by the senior authors in studying ballistic missiles (NACA RM A53D28), with the exception that radiant as well as convective heat transfer is considered in connection with glide and skip vehicles.

The ballistic vehicle is found to be the least efficient of the several types studied in the sense that it generally requires the highest velocity at the end of powered flight in order to attain a given range. This disadvantage may be offset, however, by reducing convective heat transfer to the re-entry body through the artifice of increasing pressure drag in relation to friction drag - that is, by using a blunt body. Thus the kinetic energy required by the vehicle at the end of powered flight may be reduced by minimizing the mass of coolant material involved.

The glide vehicle developing lift-drag ratios in the neighborhood of and greater than 4 is far superior to the ballistic vehicle in ability to convert velocity into range. It has the disadvantage of having far more heat convected to it; however, it has the compensating advantage that this heat can in the main be radiated back to the atmosphere. Consequently, the mass of coolant material may be kept relatively low.

The skip vehicle developing lift-drag ratios from about 1 to 4 is found to be superior to comparable ballistic and glide vehicles in converting velocity into range. At lift-drag ratios below 1 it is found to be about equal to comparable ballistic vehicles while at lift-drag ratios

~~CONFIDENTIAL~~

above 4 it is about equal to comparable glide vehicles. The skip vehicle experiences extremely large loads, however, and it encounters most severe aerodynamic heating.

As a final performance consideration, it is shown that on the basis of equal ratios of mass at take-off to mass at the end of powered flight, the hypervelocity vehicle compares favorably with the supersonic airplane for ranges in the neighborhood of and greater than one half the circumference of the earth. In the light of this and previous findings, it is concluded that the ballistic and glide vehicles have, in addition to the advantages usually ascribed to great speed, the attractive possibility of providing relatively efficient long-range flight.

Design aspects of the glide vehicle are touched on briefly. It is argued from considerations of motion and heating that vehicles of this type which fly at hypersonic speeds to impact might profitably consist of blunt-nosed bodies of revolution stabilized by a conical flare at the base and controlled by deflectable sections of the afterbody. In the event that wings are necessary to provide acceptable low-speed characteristics, it is indicated that they should have highly swept, rounded leading edges in order to alleviate the local heating problem with minimum drag penalty.

INTRODUCTION

It is generally recognized that hypervelocity vehicles are especially suited for military application because of the great difficulty of defending against them. It is also possible that for long-range operation, hypervelocity vehicles may not be overly extravagant in cost. A satellite vehicle, for example, can attain arbitrarily long range with a finite speed and hence finite energy input. E. Sanger was among the first to recognize this favorable connection between speed and range (ref. 1) and was, with Bredt, perhaps the first to exploit the speed factor in designing a long-range bomber (ref. 2). This design envisioned a rocket-boost vehicle attaining hypervelocity speeds at burnout and returning to earth along a combined skip-glide trajectory. Considerable attention was given to the propulsion and motion analysis; however, little attention was given to what is now considered to be a principal problem associated with any type of hypersonic aircraft, namely that of aerodynamic heating. In addition, the category of expendable vehicles, perhaps best characterized by the ballistic missile, was not treated.

Since the work of Sanger and Bredt there have been, of course, many treatments of long-range hypervelocity vehicles in which the propulsion, motion, and heating problems have been studied in considerable detail. However, these analyses have been devoted in the main to particular designs and are not intended to reveal, for example, the relative advantages and

disadvantages of ballistic-, skip-, and glide-type vehicles. Furthermore, it appears that the extent to which these vehicles can compete on a simple efficiency basis with lower speed aircraft of either the expendable or nonexpendable type has not been well established.

It has therefore been undertaken in the present report to make a comparative analysis of the performance of hypervelocity vehicles having ballistic, skip, and glide trajectories. An idealized propulsion system, whose performance is rather closely approached by present-day rocket motors, is assumed. The motion analysis is simplified by treating, for the most part, only optimum trajectories yielding the maximum range for a given initial kinetic energy per unit mass in the unpowered portion of flight. Aerodynamic heating is treated in a manner analogous to that employed by the senior authors in studying ballistic missiles (ref. 3) with the exception that radiant heat transfer, as well as convective heat transfer, is considered in the treatment of glide and skip vehicles. The efficiencies of these vehicles are compared with those determined by the method of Schamberg (ref. 4) for supersonic aircraft.

ANALYSIS

General Considerations

In the following analysis of long-range hypervelocity vehicles, only flight in planes containing the great circle arc between take-off and landing is considered. The flight is thought of in two phases: (a) the powered phase in which sufficient kinetic energy, as well as control, is imparted to the vehicle to bring it to a prescribed velocity, orientation, and position in space; and (b) the unpowered phase, in which the vehicle travels to its destination under the influence of gravity and aerodynamic forces.

The analyses of motion and aerodynamic heating during unpowered flight will, of necessity, differ widely for the several types of vehicles under consideration. On the other hand, motion in the powered phase is conveniently treated by a method common to all vehicles. The study of powered flight and its relation to range is therefore taken as a starting point in the analysis. The mathematical symbols employed in the analysis are listed in Appendix A.

Powered Flight and the Breguet Range Equation

In this part of the study, the following simplifying assumptions are made: (a) aerodynamic heating can be neglected on the premise that high

flight speeds are not attained until the vehicle is in the rarefied upper atmosphere;¹ (b) sufficient stability and control is available to provide proper orientation and positioning of the vehicle in space; (c) the distance traveled while under power is negligible by comparison to the overall range; and finally, (d) the thrust is very large compared to the retarding aerodynamic and gravity forces. In terms of present-day power plants, the last assumption is tantamount to assuming a rocket drive for the vehicle.

The velocity at burnout of the first stage of a multistage rocket (or the final velocity of a single-stage rocket) can then be expressed as (see, e.g., ref. 5):

$$\bar{V}_{f_1} = \frac{gI}{V_S} \ln \left(\frac{m_i}{m_{f_1}} \right) \quad (1)$$

where the initial velocity is taken as zero. In this expression, m_i and m_{f_1} represent the mass of the vehicle at the beginning and ending of first-stage flight, and $\bar{V}_{f_1} = V_{f_1}/V_S$ where $V_S = \sqrt{gr_0} = 25,930$ feet per second is the satellite velocity at the surface of the earth. The coefficient g is the acceleration due to gravity and is, along with the specific impulse I , considered constant in this phase of the analysis.² The final velocity of the vehicle at the end of the N stages of powered flight can be expressed as

$$\bar{V}_f = \bar{V}_N = \frac{gI}{V_S} \ln \left[\left(\frac{m_1}{m_{f_1}} \right) \left(\frac{m_{i2}}{m_{f_2}} \right) \cdots \left(\frac{m_{iN}}{m_{f_N}} \right) \right] \quad (2)$$

where the initial mass of any given stage differs from the final mass of the previous stage by the amount of structure, etc., jettisoned.

Now let us define an equivalent single-stage rocket having the same initial and final mass as the N -stage rocket and the same initial and final velocity. There is, then, an effective specific impulse defined by

¹This assumption is in the main permissible. A possible exception occurs, however, with the glide vehicle for which heat-transfer rates near the end of powered flight can be comparable to those experienced in unpowered gliding flight.

²Both g and I actually vary with altitude, of course, but for the powered flight trajectories of interest here the variations are small and it is permissible to use constant average values of these quantities.

$$I_e = I \frac{\ln \left[\left(\frac{m_1}{m_{f1}} \right) \left(\frac{m_{12}}{m_{f2}} \right) \cdots \left(\frac{m_{1N}}{m_{fN}} \right) \right]}{\ln \left(\frac{m_1}{m_f} \right)} \quad (3)$$

whereby equation (2) can be written as

$$\bar{V}_f = \frac{g I_e}{V_S} \ln \left(\frac{m_1}{m_f} \right) \quad (4)$$

The effective specific impulse I_e is always somewhat less than the actual specific impulse, but for an efficient design they are very nearly equal. Throughout the remainder of the analysis the effective impulse I_e will be used.

Equation (4) might be termed the "ideal power plant" equation for accelerated flight because, when considered in combination with the assumptions underlying its development, attention is naturally focused on the salient factors leading to maximum increase in velocity for given expenditure of propellant. Thus the thrust acts only in overcoming inertia forces, and the increase in vehicle velocity is directly proportional to the exhaust velocity (gI) for the propellant.

Now we recognize that an essential feature of the hypervelocity vehicles under study here is that they use their velocity (or kinetic energy per unit mass) to obtain range. For this reason, equation (4) also constitutes a basic performance equation for these vehicles because it provides a connecting link between range requirements and power-plant requirements.

In addition to comparing various types of hypervelocity vehicles, our attention will also be focused upon comparison of these vehicles with lower speed, more conventional types of aircraft. For this purpose it is useful to develop an alternate form of equation (4). We observe that the kinetic energy imparted to the vehicle is

$$\frac{1}{2} m_f V_f^2$$

This energy is equated to an effective work done, defined as the product of the range traveled and a constant retarding force. (Note that the useful kinetic energy at the end of powered flight is zero.) This force is termed the "effective drag" D_e . Thus

$$D_e R = \frac{1}{2} m_f V_f^2 \quad (5)$$

where R is flight range measured along the surface of the earth. Similarly, we may define an "effective lift" L_e , equal to the final weight of the vehicle

$$L_e = W_f = m_f g$$

from which it follows that equation (5) may be written as

$$R = \left(\frac{L}{D}\right)_e \frac{V_f^2}{2g} \quad (6)$$

where $(L/D)_e$ is termed the "effective lift-drag ratio." Combining equations (4) and (6), we obtain

$$R = \left(\frac{L}{D}\right)_e I_e V_e \ln \left(\frac{m_i}{m_f}\right) \quad (7)$$

where

$$V_e = \frac{V_f}{2} \quad (8)$$

and represents an "effective" flight velocity of the vehicle. Equation (7) will prove useful in comparing hypersonic vehicles with conventional aircraft because of its analogy to the Breguet range equation,

$$R = \frac{L}{D} IV \ln \left(\frac{m_i}{m_f}\right) \quad (9)$$

It will also prove useful to have equation (7) in the dimensionless form obtained by dividing through with r_0 , the radius of the earth. In this case we have

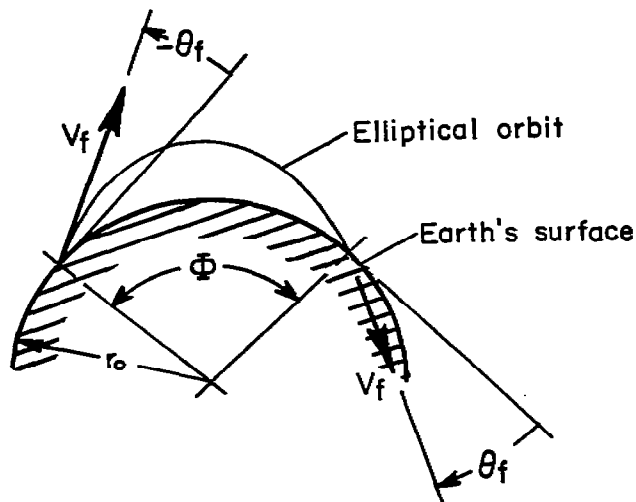
$$\Phi = \frac{R}{r_0} = \left(\frac{L}{D}\right)_e \bar{V}_e \left(\frac{g I_e}{V_s}\right) \ln \left(\frac{m_i}{m_f}\right) \quad (10)$$

where Φ is the range in radians of arc traversed along the surface of the earth.

Motion in Unpowered Flight

Ballistic trajectory.- In studying the motion of long-range vehicles in this trajectory, advantage is taken of the fact that the traverse through the earth's atmosphere generally forms only a small part of the total trajectory. Therefore, the deflection and deceleration encountered in the re-entry phase (discussed in detail in ref. 3) are neglected in

the computation of the total range. With the added simplification that the contribution to range of the powered phase of flight is negligible, the ballistic trajectory becomes one of Kepler's planetary ellipses, the major axis of which bisects the total angle of arc Φ traveled around the earth (see sketch). For the trajectories of interest here ($\bar{V}_f \leq 1$), the far focus of the ellipse is at the mass center of the earth. For purposes of range computation, then, the ballistic vehicle leaves and returns to the earth's surface at the same absolute magnitude of velocity and incidence³ (see sketch).



The expression for range follows easily from the equation of the ellipse (see, e.g., ref. 6) and can be written

$$\Phi = \frac{R}{r_0} = 2 \tan^{-1} \left(\frac{\sin \theta_f \cos \theta_f}{\frac{1}{\bar{V}_f^2} - \cos^2 \theta_f} \right) \quad (11)$$

where the angle of incidence θ_f is considered positive. In order to determine the optimum trajectory giving maximum range for a given velocity V_f , equation (11) is differentiated with respect to θ_f and equated to 0, yielding

$$\left. \begin{aligned} \bar{V}_f^2 = \frac{V_f^2}{V_S^2} &= 1 - \tan^2 \theta_f \\ \Phi = \frac{R}{r_0} &= \pi - 4\theta_f \end{aligned} \right\} \quad (12)$$

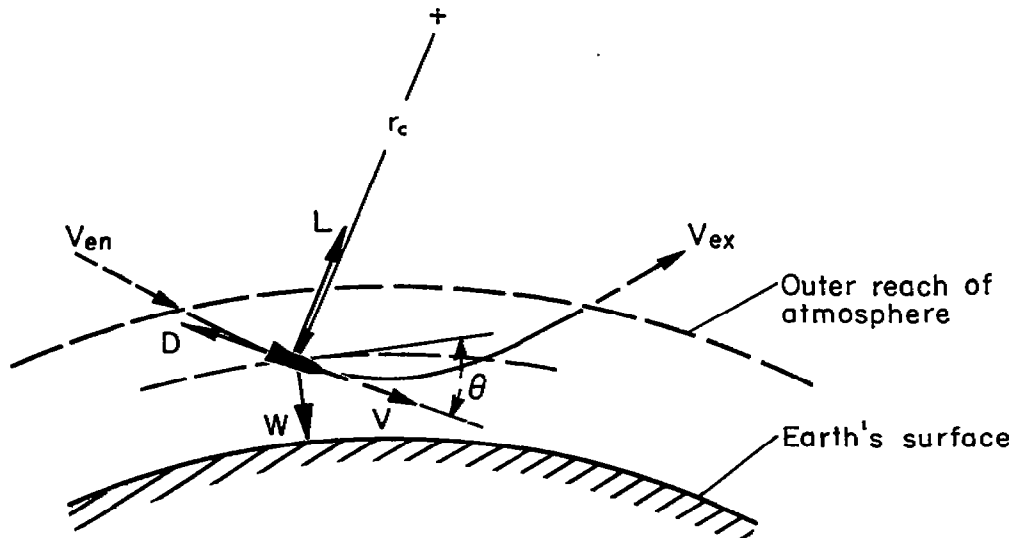
³Rotation of the earth is neglected in this and all other phases of the analysis.

Equations (11) and (12) have been employed to determine velocity as a function of incidence for various values of range and the results are presented in figure 1.⁴ The "minimum velocity line" of figure 1 corresponds to the optimum trajectories (eqs. (12)).

The effective lift-drag ratios can easily be calculated for optimum ballistic vehicles using equation (6) in combination with the information of figure 1. The required values of $(L/D)_e$ as a function of range are presented in figure 2.

Skip trajectory.- This trajectory can be thought of as a succession of ballistic trajectories, each connected to the next by a "skipping phase" during which the vehicle enters the atmosphere, negotiates a turn, and is then ejected from the atmosphere. The motion analysis for the ballistic missile can, of course, be applied to the ballistic phases of the skip trajectory. It remains, then, to analyze the skipping phases and to combine this analysis with the ballistic analysis to determine over-all range.

To this end, consider a vehicle in the process of executing a skip from the atmosphere (see sketch).



⁴Independent calculations of ballistic trajectories by King-Hele and Gilmore (ref. 7) came to the attention of the authors after completion of this analysis. The results presented here agree with those of reference 7.

The parametric equations of motion in directions perpendicular and parallel to the flight path s are, respectively,

$$\left. \begin{aligned} C_L \frac{\rho V^2}{2} A - mg \cos \theta &= \frac{mV^2}{r_c} \\ -C_D \frac{\rho V^2}{2} A + mg \sin \theta &= m \frac{dV}{dt} \end{aligned} \right\} \quad (13)$$

where r_c is the local radius of curvature of the flight path, θ is the local inclination to the horizontal (positive downward), ρ is the local air density, and C_L and C_D are the lift and drag coefficients, respectively, based on the reference area, A , of the aircraft.

In the turning process, aerodynamic lift must obviously predominate over the gravity component, $mg \cos \theta$. By analogy to the atmospheric re-entry of ballistic missiles (see ref. 3), aerodynamic drag generally predominates over the gravity component, $mg \sin \theta$. Moreover, the integrated contribution to velocity of this gravity component during descent in a skip is largely balanced by an opposite contribution during ascent. For these reasons we will idealize the analysis by neglecting gravity entirely.⁵ In this case equations (13) reduce to

$$\left. \begin{aligned} \frac{1}{2} C_L \rho V^2 A &= -mV^2 \frac{d\theta}{ds} \\ -\frac{1}{2} C_D \rho V^2 A &= m \frac{dV}{dt} \end{aligned} \right\} \quad (14)$$

where $d\theta/ds = -\frac{1}{r_c}$ to the accuracy of this analysis.

Now we assume an isothermal atmosphere, in which case

$$\rho = \rho_0 e^{-\beta y} \quad (15)$$

where ρ_0 and β are constants, and $y = (r - r_0)$ is the altitude from sea level (see ref. 3 for discussion of accuracy of this assumption).

⁵This approach is analogous to the classical treatment of impact problems in which all forces exclusive of impact forces (aerodynamic forces in this case) are neglected as being of secondary importance. Gravity is shown to be of secondary importance in figure 3 where the trajectory results obtainable from equations (13) and (14) are presented for the first skipping phase of an $L/D = 2$, $\Phi = 1$ skip missile.

Noting that $dy/ds = -\sin \theta$, we combine the first of equations (14) with equation (15) to yield

$$\frac{C_L \rho_0 A}{2m} e^{-\beta y} dy = \sin \theta d\theta \quad (16)$$

This expression can be integrated to give

$$\frac{C_L \rho_0 A}{2\beta m} e^{-\beta y} = \cos \theta - \cos \theta_{en} \quad (17)$$

where ρ is taken as zero at the altitude corresponding to the effective "outer reach" of the atmosphere. Equation (17) points out an important feature of the skip path; namely, $\cos \theta$ is a single-valued function of altitude. Since θ proceeds from positive to negative values, it is evident that

$$\theta_{en_{n-1}} = -\theta_{ex_n} \quad (18)$$

where the subscripts en and ex refer to atmospheric entrance and exit conditions, respectively, and the numbers $n-1$ and n refer to successive ballistic phases of the trajectory. Now since

$$\frac{dv}{dt} = v \frac{dv}{ds} = \frac{1}{2} \frac{dv^2}{ds}$$

equations (14) may be combined to obtain

$$\frac{1}{2} \frac{dv^2}{ds} = \frac{v^2}{L/D} \frac{d\theta}{ds} \quad (19)$$

which, for constant L/D , can be integrated to yield

$$\frac{v_{ex_n}}{v_{en_{n-1}}} = e^{\frac{\theta_{ex_n} - \theta_{en_{n-1}}}{L/D}} \quad (20)$$

With the aid of equation (18), this expression may be written

$$\frac{V_{ex_n}}{V_{en_{n-1}}} = e^{-\frac{2\theta_{en_{n-1}}}{L/D}} \quad (21)$$

which relates the velocities at the beginning and end of a skip to the lift-drag ratio and the entrance angle of the vehicle to the earth's atmosphere. From equation (18) it follows further that the entrance angle for each skip in the trajectory is the same, so that

$$\theta_{en_n} = \theta_{en_{n-1}} = \dots = \theta_f$$

and hence equation (21) becomes

$$\frac{V_{ex_n}}{V_{en_{n-1}}} = e^{-\frac{2\theta_f}{L/D}} \quad (22)$$

We now combine this result of the skip analysis with that of the ballistic analysis to obtain the total flight range. From equation (11), the range of the nth ballistic segment of the trajectory is

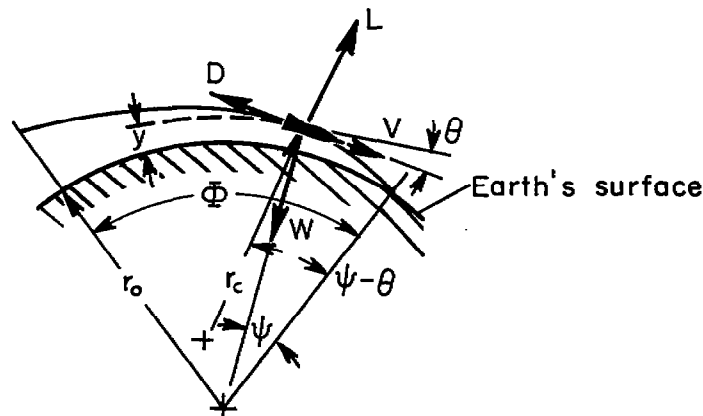
$$\varphi_n = 2 \tan^{-1} \left[\frac{\sin \theta_f \cos \theta_f}{\left(\frac{V_S}{V_{ex_n}} \right)^2 - \cos^2 \theta_f} \right] \quad (23)$$

Consistent with the idealization of the skipping process as an impact problem, we neglect the contribution to range of each skipping phase so that the total range is simply the sum of the ballistic contributions. From equations (22) and (23) this range is then

$$\phi = \frac{R}{r_0} = \sum_{n=0}^{\infty} \varphi_n = 2 \sum_{n=0}^{\infty} \tan^{-1} \left(\frac{\sin \theta_f \cos \theta_f}{\frac{4n\theta_f}{e \frac{L/D}{V_f^2}} - \cos^2 \theta_f} \right) \quad (24)$$

From this expression we see that for any given velocity at the end of powered flight there is a definite skipping angle which maximizes the range of an aircraft developing a particular lift-drag ratio. These skipping angles have been obtained with the aid of an IBM CPC, and the corresponding values of \bar{V}_f as a function of range for various L/D are presented in figure 4. Corresponding values of $(L/D)_e$ have been obtained using equation (6) and the results are shown in figure 5.

Glide trajectory.- The trajectory of the glide vehicle is illustrated in the accompanying sketch. As in the previous analyses, the distance covered in the powered phase will be neglected in the determination of total range.



The parametric equations of motion normal and parallel to the direction of motion are the relations of equations (13) rewritten in the form

$$\left. \begin{aligned} L - mg \cos \theta &= - \frac{mV^2}{r_c} \\ -D + mg \sin \theta &= m \frac{dV}{dt} \end{aligned} \right\} \quad (25)$$

Under the assumption of small inclination angle θ to the horizontal (thus $\cos \theta \approx 1$, $\sin \theta \approx \theta$), constant gravity acceleration (i.e., $\frac{r}{r_o} \approx 1$), and noting the following relations

$$\left. \begin{aligned} \frac{dV}{dt} &= V \frac{dV}{ds} = \frac{1}{2} \frac{dV^2}{ds} \\ \frac{1}{r_c} &= \frac{d(\psi - \theta)}{ds} \\ \frac{d\psi}{ds} &= \frac{\cos \theta}{r} \approx \frac{1}{r_0} \end{aligned} \right\} \quad (26)$$

equations (25) can be written in the forms

$$\left. \begin{aligned} L &= mV^2 \frac{d\theta}{ds} + mg - \frac{mV^2}{r_0} \\ D &= -\frac{1}{2} m \frac{dV^2}{ds} + mg \theta \end{aligned} \right\} \quad (27)$$

Dividing the first of equations (27) by the second yields the following differential equation

$$g \left(1 - \frac{L}{D} \theta \right) + \left(\frac{1}{2} \frac{L}{D} \frac{dV^2}{ds} + V^2 \frac{d\theta}{ds} \right) - \frac{V^2}{r_0} = 0 \quad (28)$$

But, as is demonstrated in Appendix B, the terms $\frac{L}{D} g\theta$ and $V^2 \frac{d\theta}{ds}$ may be neglected so that equation (28) reduces to

$$\frac{dV^2}{ds} - \frac{2}{r_0(L/D)} V^2 + \frac{2g}{L/D} = 0 \quad (29)$$

Since

$$V_s^2 = gr_0$$

equation (29) can be integrated for constant $\frac{L}{D}$ to give the velocity in nondimensional form as

$$\bar{V}^2 = 1 - (1 - \bar{V}_f^2) e^{\frac{2\phi}{L/D}} \quad (30)$$

This expression gives velocity as a function of range for what Sanger (ref. 2) has termed the equilibrium trajectory - that is, the trajectory for which the gravity force is essentially balanced by the aerodynamic lift and centrifugal force, or

$$\frac{L}{W} \approx 1 - \bar{V}^2 \quad (31)$$

It follows from equation (25) that velocity can be expressed in the form

$$\bar{V}^2 = \frac{1}{1 + \frac{C_{LAVS^2\rho}}{2mg}} \quad (32)$$

Now it is intuitively obvious that as the maximum range is approached, $L/W \rightarrow 1$ and hence \bar{V}^2 becomes small compared to one (see eq. (31)). In this event it follows from equation (30) that the maximum range for the glide vehicle is given by

$$\phi = \frac{R}{r_0} = \frac{1}{2} \left(\frac{L}{D} \right) \ln \left(\frac{1}{1 - \bar{V}_f^2} \right) \quad (33)$$

The relation between velocity and range has been determined with equation (33) for various values of L/D and the results are presented in figure 6. Corresponding values of $(L/D)_e$ have been obtained using equation (6) and are presented in figure 7.

These considerations complete the motion analysis and attention is now turned to the aerodynamic heating of the several types of vehicles under consideration.

Heating in Unpowered Flight

General considerations. - Three aspects of the aerodynamic heating of hypervelocity vehicles will be treated here; namely,

1. The total heat input
2. The maximum time rate of average heat input per unit area
3. The maximum time rate of local heat input per unit area

Total heat input is, of course, an important factor in determining over-all coolant weight, whether the coolant be solid (e.g., the structure), liquid, or gas, or a combination thereof. The maximum time rate of average heat input per unit area can determine peak average flow rates in the case of fluid coolants and may dictate over-all structural strength in the event that thermal stresses predominate.

Excessive local heating is, of course, a serious problem with hypervelocity vehicles. This problem may vary depending upon the type of the vehicle. Thus, for the ballistic vehicle, an important local "hot spot" is the stagnation region of the nose, while for the skip or glide vehicle attention may also be focused on the leading edges of planar surfaces used for developing lift and obtaining stable and controlled flight. In this analysis attention is, for the purpose of simplicity, restricted to the "hot spot" at the nose. In particular, we consider the maximum time rate of local heat input per unit area because of its bearing on local coolant flow rates and local structural strength.

It is undertaken to treat only convective heat transfer at this stage of the study. As will be demonstrated, radiant heat transfer from the surface should not appreciably influence convective heat transfer to a vehicle. Therefore, alleviating effects of radiation are reserved for attention in the discussion of particular vehicles later in the paper. This analysis is further simplified by making the assumptions that

1. Effects of gaseous imperfections may be neglected
2. Shock-wave boundary-layer interaction may be neglected
3. Prandtl number is unity
4. Reynolds analogy is applicable

These assumptions are obviously not permissible for an accurate quantitative study of a specific vehicle. Nevertheless they should not invalidate this comparative analysis which is only intended to yield information of a general nature regarding the relative merits and problems of different types of vehicle (see ref. 3 for a more complete discussion of these assumptions in connection with ballistic vehicles).

In calculating convective heat transfer to hypervelocity vehicles, the theoretical approach taken in reference 3 for ballistic vehicles is, up to a point, quite general and can be employed here. Thus, on the basis of the foregoing assumptions, it follows that for large Mach numbers, the difference between the local recovery temperature and wall temperature can be expressed as

$$(T_r - T_w)_L = \frac{V^2}{2C_p} \quad (34)$$

where T_r is the recovery temperature, T_w is the wall temperature, C_p is the specific heat at constant pressure, and the subscript l denotes local conditions at a point on the surface.

It is clear, however, that the walls of a vehicle should be maintained sufficiently cool to insure structural integrity. It follows in this case that, the recovery temperature at hypervelocities will be large by comparison to the wall temperature and equation (34) may be simplified to read

$$T_{r_l} = \frac{V^2}{2C_p} \quad (35)$$

To the accuracy of this analysis, then, the convective heat transfer is independent of wall temperature. Therefore, as previously asserted, radiant heat transfer should not appreciably influence convective heat transfer and the one can be studied independently of the other.

Now, according to Reynolds analogy, the local heat-transfer coefficient h_l is, for a Prandtl number of unity, given by the expression

$$h_l = \frac{1}{2} C_{F_l} C_{p_l} \rho_l V_l \quad (36)$$

where C_{F_l} is the local skin-friction coefficient based on conditions just outside the boundary layer. With the aid of equations (35) and (36) the time rate of local heat transfer per unit area,

$$\frac{dH}{dt} = h_l (T_r - T_w)_l \quad (37)$$

can be written as

$$\frac{dH}{dt} = \frac{V^2}{4C_p} \left(C_{F_l} C_{p_l} \rho_l V_l \right) \quad (38)$$

Equation (38) can be integrated over the surface of a body to yield the time rate of total heat input as follows

$$\frac{dQ}{dt} = \int_S \frac{dH}{dt} dS = \frac{1}{4} \rho V^3 C_F S \quad (39)$$

wherein C_{p_l} is set equal to C_p and

$$C_F' = \frac{1}{S} \int_S C_{F_l} \frac{\rho_l}{\rho} \frac{V_l}{V} dS \quad (40)$$

The parameter C_F' is termed the "equivalent skin-friction coefficient" and will be assumed constant for a particular vehicle. From equation (39) we can obtain two alternate forms which will prove useful; namely, the altitude rate of total heat input defined by

$$\frac{dQ}{dy} = \frac{1}{V \sin \theta_f} \frac{dQ}{dt} = \frac{\rho V^2 C_F' S}{4 \sin \theta_f} \quad (41)$$

and the range rate of total heat input defined as

$$\frac{dQ}{d(r_0 \phi)} = \frac{1}{V \cos \theta_f} \frac{dQ}{dt} = \frac{\rho V^2 C_F' S}{4 \cos \theta_f} \quad (42)$$

The total heat input may be obtained by integration of equations (39), (41) or (42), depending upon the particular variable used.

The time rate of average heat input per unit area may be obtained from equation (39) as

$$\frac{dH_{av}}{dt} = \frac{1}{S} \frac{dQ}{dt} = \frac{1}{4} \rho V^3 C_F' \quad (43)$$

Consider next the local convective heat transfer in the region of the nose. The time rate of local heat input per unit area was determined in reference 3 under the assumptions that viscosity coefficient varies as the square root of the absolute temperature, and that flow between the bow shock wave and the stagnation point is incompressible. In this case it was found that⁶

⁶While this expression is no doubt in error due to neglecting compressibility effects, nevertheless it is a useful guide in studying the local heat-transfer problem. (See ref. 3 for more complete discussion of this matter.)

$$\frac{dH_s}{dt} = 6.8 \times 10^{-6} \sqrt{\frac{\rho}{\sigma}} v^3 \quad (44)$$

where σ is the radius of curvature of the body at the stagnation point.

With these relations we are now in a position to study the heating of the several types of vehicles of interest.

Ballistic vehicle.- The heating for this case has already been analyzed in reference 3. Only the results will be given here.

The ratio of the total heat input to the initial kinetic energy was found to be

$$\frac{Q}{\frac{1}{2} m V_f^2} = \frac{1}{2} \frac{C_F' S}{C_D A} \left(1 - e^{-\frac{C_D \rho_0 A}{\beta m \sin \theta_f}} \right) \quad (45)$$

For the "relatively light missile," which is of principal interest here,

$$e^{-\frac{C_D \rho_0 A}{\beta m \sin \theta_f}} \ll 1 \quad (46)$$

and equation (45) reduces to

$$\frac{Q}{\frac{1}{2} m V_f^2} = \frac{1}{2} \frac{C_F' S}{C_D A} \quad (47)$$

The time rate of average heat input per unit area was found to be

$$\frac{dH_{av}}{dt} = \frac{1}{S} \frac{dQ}{dt} = \frac{C_F' \rho_0 V_f^3}{4} e^{-\beta y} e^{-\frac{3 C_D \rho_0 A}{2 \beta m \sin \theta_f}} e^{-\beta y} \quad (48)$$

which has the maximum value

$$\left(\frac{dH_{av}}{dt} \right)_{\max} = \left(\frac{dH_{av}}{dt} \right)_{y_a} = \frac{\beta}{6e} \frac{C_F'}{C_D A} m V_f^3 \sin \theta_f \quad (49)$$

at the altitude

$$y_a = \frac{1}{\beta} \ln \left(\frac{3C_D \rho_o A}{2\beta m \sin \theta_f} \right) \quad (50)$$

Equation (49) applies, of course, only if the altitude of occurrence is above ground level. If the value of y_a is negative then the maximum rate will, of course, occur at sea level.

The time rate of local heat input per unit area to the stagnation region of the nose was found to be

$$\frac{dH_s}{dt} = 6.8 \times 10^{-6} \sqrt{\frac{\rho_o}{\sigma}} V_f^3 e^{-\frac{\beta y}{2}} e^{-\frac{3C_D \rho_o A}{2\beta m \sin \theta_f}} e^{-\beta y} \quad (51)$$

having a maximum value of

$$\left(\frac{dH_s}{dt} \right)_{\max} = \left(\frac{dH_s}{dt} \right)_{y_b} = 6.8 \times 10^{-6} \sqrt{\frac{\beta m \sin \theta_f}{3eC_D \sigma A}} V_f^3 \quad (52)$$

occurring at the altitude

$$y_b = \frac{1}{\beta} \ln \left(\frac{3C_D \rho_o A}{\beta m \sin \theta_f} \right) \quad (53)$$

If the value of y_b is negative, then the maximum value occurs at ground level.

Skip vehicle.- With the aid of equation (17), the density at any point in a given skipping phase is found to be

$$\rho = \rho_o e^{-\beta y} = \frac{2\beta m}{C_L A} (\cos \theta - \cos \theta_f) \quad (54)$$

where it is to be recalled that $\theta_{en} = \theta_f$. The corresponding velocity is obtained by integrating equation (19) for constant L/D , yielding

$$V = V_{en} e^{-\frac{\theta_f - \theta}{L/D}} \quad (55)$$

By substitution of equations (54) and (55) into equation (39), the time rate of total heat input at any point in a skipping phase can be expressed as follows:

$$\frac{dQ}{dt} = \frac{1}{2} \frac{C_F S}{C_D A} \frac{\beta m}{L/D} V_{en}^3 (\cos \theta - \cos \theta_f) e^{-\frac{3(\theta_f - \theta)}{L/D}} \quad (56)$$

Now, recalling that $ds/dt = V$, the first of equations (14) may be combined with equation (17) to yield

$$\frac{d\theta}{dt} = -\beta V (\cos \theta - \cos \theta_f) \quad (57)$$

Inasmuch as $V_{en} = V_{ex}$ for any ballistic phase, it then follows from equation (22) that

$$\frac{(V_{en})_n}{(V_{en})_{n=1}} = \frac{(V_{en})_n}{V_f} = e^{-(n-1) \frac{2\theta_f}{L/D}} \quad (58)$$

With the aid of equations (57) and (58), equation (56) can be integrated to give the total heat input for a given skipping phase. Thus we obtain

$$\frac{Q_n}{\frac{1}{2} m V_f^2} = \frac{1}{2} \frac{C_F S}{C_D A} \left(1 - e^{-\frac{2\theta_f}{L/D}} \right) e^{-(n-1) \frac{2\theta_f}{L/D}} \quad (59)$$

where n refers to the ballistic phase subsequent to the given skipping phase.

The total heat input for the entire trajectory can be obtained by summing up the heat inputs for each separate skipping phase. Performing this operation yields

$$\frac{Q}{\frac{1}{2} m V_f^2} = \sum_{n=1}^{\infty} \frac{Q_n}{\frac{1}{2} m V_f^2} = \frac{1}{2} \frac{C_F' S}{C_D A} \left(1 - e^{-\frac{4\theta_f}{L/D}} \right) \sum_{n=1}^{\infty} e^{-(n-1) \frac{4\theta_f}{L/D}} \quad (60)$$

The summation on the right side of equation (60) represents a geometric series which can readily be evaluated. The total heat input for the entire trajectory then becomes

$$\frac{Q}{\frac{1}{2} m V_f^2} = \frac{1}{2} \frac{C_F' S}{C_D A} \quad (61)$$

which is identical to the result obtained for the light ballistic missile (eq. (47)).

The time rate of average heat input per unit area is obtained by dividing equation (56) with the surface area, thus yielding

$$\frac{dH_{av}}{dt} = \frac{1}{2} \frac{C_F'}{C_D A} \frac{\beta m}{L/D} V_{en}^3 (\cos \theta - \cos \theta_f) e^{-\frac{s(\theta_f - \theta)}{L/D}} \quad (62)$$

It can be shown that this expression has a peak value at a point in the skip, θ_a , given by

$$(\cos \theta_a - \cos \theta_f) = \frac{L/D}{3} \sin \theta_a$$

or

$$\theta_a = \tan^{-1} \frac{3}{L/D} - \sin^{-1} \frac{\cos \theta_f}{\sqrt{1 + \left(\frac{L/D}{3}\right)^2}} \quad (63)$$

From equation (22) it can be concluded that the maximum heat-transfer rate will occur in the first skip where $V_{en} = V_f$; consequently,

$$\left(\frac{dH_{av}}{dt}\right)_{\max} = \frac{\beta m}{6} \frac{C_F'}{C_{DA}} V_f^3 \sin \theta_a e^{-\frac{3(\theta_f - \theta_a)}{L/D}} \quad (64)$$

The time rate of local heat input per unit area in the stagnation region of the nose is obtained by introducing equations (54) and (55) into equation (44) with the following result:

$$\frac{dH_s}{dt} = 6.8 \times 10^{-8} \left(\frac{2\beta m}{C_{LA}\sigma}\right)^{1/2} (\cos \theta - \cos \theta_f)^{1/2} V_{en}^3 e^{-\frac{3(\theta_f - \theta)}{L/D}} \quad (65)$$

Equation (65) has a peak value at a point θ_b in a skip given by

$$(\cos \theta_b - \cos \theta_f) = \frac{L/D}{6} \sin \theta_b$$

or

$$\theta_b = \tan^{-1} \frac{6}{L/D} - \sin^{-1} \frac{\cos \theta_f}{\sqrt{1 + \left(\frac{L/D}{6}\right)^2}} \quad (66)$$

It is clear in this case also that the heat-transfer rate will have its maximum value in the first skipping phase where the velocities are highest. Since $V_{en} = V_f$ in the first skip, equation (65) becomes

$$\left(\frac{dH_s}{dt}\right)_{\max} = 6.8 \times 10^{-8} \left(\frac{\beta m L/D \sin \theta_b}{3C_{LA}\sigma}\right)^{1/2} V_f^3 e^{-\frac{3(\theta_f - \theta_b)}{L/D}} \quad (67)$$

Glide vehicle.- From equations (30) and (32), the density at a point in the glide trajectory is found to be

$$\rho = \frac{2mg}{C_{LAVS}^2} \frac{(1 - \bar{V}_f^2) e^J}{1 - (1 - \bar{V}_f^2) e^J} \quad (68)$$

where

$$J = \frac{2q}{L/D}$$

By substitution of equations (30) and (68) into equation (39), the time rate of total heat input can be expressed as

$$\frac{dQ}{dt} = \frac{1}{2} \frac{C_F'S}{C_D A} \frac{mg\bar{V}_S}{L/D} (1 - \bar{V}_f^2) e^J \left[1 - (1 - \bar{V}_f^2) e^J \right]^{1/2} \quad (69)$$

Now with the aid of equations (30) and (33), equation (69) can be integrated over the limits of the glide trajectory to yield the total heat input in terms of the initial kinetic energy as

$$\frac{Q}{\frac{1}{2} m \bar{V}_f^2} = \frac{1}{2} \frac{C_F'S}{C_D A} \quad (70)$$

which expression is identical with that obtained for the skip vehicle (eq. (61)) and for the light ballistic vehicle (eq. (47)).

Now the time rate of average heat input per unit area is found by dividing equation (69) with the surface area, thus yielding

$$\frac{dH_{av}}{dt} = \frac{1}{2} \frac{C_F'S}{C_D A} \frac{mg\bar{V}_S}{L/D} (1 - \bar{V}_f^2) e^J \left[1 - (1 - \bar{V}_f^2) e^J \right]^{1/2} \quad (71)$$

It follows from this expression that the maximum time rate of average heat input per unit area is

$$\left(\frac{dH_{av}}{dt}\right)_{\max} = \left(\frac{dH_{av}}{dt}\right)_{J_a} = \frac{1}{3\sqrt{3}} \frac{C_F'}{C_{DA}} \frac{mgV_S}{L/D} \quad (72)$$

at a value J_a given by

$$J_a = -\ln \frac{3}{2} (1 - \bar{V}_f^2) \quad (73)$$

If J_a is taken as a reference value, and equations (71) and (72) expressed in terms of J_a and incremental changes $\Delta J = J - J_a$, it can easily be shown that

$$\frac{dH_{av}/dt}{(dH_{av}/dt)_{\max}} = e^{\Delta J} (3 - 2e^{\Delta J})^{1/2} = F_a(\Delta J) \quad (74)$$

The dependence of $F_a(\Delta J)$ on ΔJ is shown in figure 8.⁷

The velocity at which the maximum average heat input rate occurs can be obtained by substituting equation (73) into equation (30) yielding

$$\bar{V} = \frac{1}{\sqrt{3}} \quad (75)$$

In equation (30) it is seen that the velocity is greatest at the start of unpowered flight (i.e., when $J = 0$). Equations (72), (73), and (74) apply, therefore, only when $\bar{V}_f \geq (1/\sqrt{3})$.

For cases when $\bar{V}_f \leq (1/\sqrt{3})$, the maximum time rate of average heat input per unit area will occur at the start of unpowered flight and is given by

$$\left(\frac{dH_{av}}{dt}\right)_{\max} = \left(\frac{dH_{av}}{dt}\right)_{J_a=0} = \frac{1}{2} \frac{C_F'}{C_{DA}} \frac{mgV_S}{L/D} (1 - \bar{V}_f^2) \bar{V}_f \quad (76)$$

⁷Similar generalized curves have been obtained for ballistic vehicles in reference 3.

The maximum time rate of local heat input per unit area in the stagnation region of the nose is found by first substituting equations (30) and (68) into equation (44) to obtain

$$\frac{dH_s}{dt} = 6.8 \times 10^{-8} \sqrt{\frac{2mg}{C_L A \sigma}} V_S^2 \left[1 - (1 - \bar{V}_f^2) e^J \right] \left[(1 - \bar{V}_f^2) e^J \right]^{1/2} \quad (77)$$

The maximum time rate is then

$$\left(\frac{dH_s}{dt} \right)_{\max} = \left(\frac{dH_s}{dt} \right)_{J_b} = \frac{2}{3\sqrt{3}} 6.8 \times 10^{-8} \sqrt{\frac{2mg}{C_L A \sigma}} V_S^2 \quad (78)$$

occurring at a value of J_b given by

$$J_b = -\ln 3(1 - \bar{V}_f^2) \quad (79)$$

With J_b as a reference, it can easily be shown that

$$\frac{dH_s/dt}{(dH_s/dt)_{\max}} = \frac{1}{2} e^{\frac{\Delta J}{2}} \left(3 - e^{\Delta J} \right) = F_b(\Delta J) \quad (80)$$

where

$$\Delta J = J - J_b$$

The dependence of $F_b(\Delta J)$ on ΔJ is shown in figure 8.

With reference to equations (30) and (74) it can be seen that the maximum time rate of local heat transfer in the stagnation region occurs when

$$\bar{V} = \sqrt{\frac{2}{3}} \quad (81)$$

It is apparent then that equations (77), (78), and (79) apply only when $\bar{V}_f \geq \sqrt{2/3}$. For cases where $\bar{V}_f \leq \sqrt{2/3}$, the maximum time rate of local heat input per unit area will occur at the start of unpowered flight and is given by

$$\left(\frac{dH_s}{dt}\right)_{\max} = \left(\frac{dH_s}{dt}\right)_{J_p=0} = 6.8 \times 10^{-8} \sqrt{\frac{2mg}{C_L A \sigma}} V_s^2 \bar{V}_f^2 (1 - \bar{V}_f^2)^{1/2} \quad (82)$$

DISCUSSION

Performance of Hypervelocity Vehicles

In this study the point of view is taken that the performance of long-range hypervelocity vehicles is measured by their efficiency of flight. Thus, for example, it is presumed that the advantages (military and otherwise) of short time of flight accrue equally to all vehicles.

The efficiency of flight is perhaps best measured by the cost of delivering a given pay load a given range - the higher the cost, the lower the efficiency. Quite obviously it is far beyond the scope of the present paper to actually compute this cost. Rather, then, we adopt a more accessible parameter of hypervelocity flight, namely, the initial mass of the vehicle, as a measure of cost. In effect, then, the assumption is made that the higher the initial mass of a vehicle the higher the cost and the lower the efficiency. With these thoughts in mind, it is constructive to reconsider the basic performance equation (eq. (4)) written in the form

$$m_i = m_{pe} \frac{V_f}{g I_e} \quad (83)$$

This expression clearly demonstrates the roles played by the three factors which influence the initial mass of a vehicle required to travel a given range. For one thing there is the power plant, and as we would expect, increasing the effective specific impulse increases the over-all efficiency of flight in the sense that it tends to reduce the initial mass. The velocity at burnout influences initial mass by dictating the amount of fuel required, and it is not surprising that decreasing the required burnout velocity (e.g., by increasing the L/D of a skip or glide vehicle) tends to decrease the initial mass. Finally, we see that the initial mass is proportional to the final mass which consists of the pay load, structure (and associated equipment), and coolant. If we presume the mass of the pay load to be some fixed quantity, then the initial mass will vary in accordance with this mass of structure and coolant.

Now we assume for comparative purposes that the power plant for one vehicle is equally as good as the power plant for another vehicle - that is to say I_e is a more or less fixed quantity. In this event it is permissible to restrict our attention to two main performance considerations; namely, the prescribed motion as it influences the required burnout velocity, and the resulting aerodynamic heating as it influences structure and coolant. We therefore proceed to discuss the comparative performance of long-range hypervelocity vehicles in terms of these considerations.

Motion.- The dependence of burnout velocity V_f on range was determined in the analysis of motion in unpowered flight and the results obtained for the several types of hypervelocity vehicle under study were presented in figures 1, 4, and 6. Using these results in combination with the basic performance equation we have calculated the corresponding initial to final mass ratios m_i/m_f as a function of range. For these and subsequent calculations it has been assumed that the rocket power plant develops an effective specific impulse of 225 seconds.⁸ The results of these calculations are presented in figure 9 and we observe that, in general, the mass ratios are highest for the ballistic vehicle. The glide and skip vehicles have comparable and relatively low mass ratios at lift-drag ratios in the neighborhood of 4 and greater. The skip vehicle is superior, however, to the glide vehicle at lift-drag ratios in the neighborhood of 2. From considerations of motion alone, then, we conclude that the skip vehicle and the glide vehicle developing lift-drag ratios greater than 2 are superior efficiencywise, in the sense of this report, to the ballistic vehicle. Let us now determine how these observations are modified by considerations of aerodynamic heating.

Aerodynamic heating.- The analysis has revealed one particularly salient factor in regard to the heat transferred by convection to hypervelocity vehicles that expend the majority of their kinetic energy of flight in traveling through the earth's atmosphere. This factor is that the amount of kinetic energy which appears in the body in the form of heat is proportional to the ratio of friction force to total drag force acting on the body (see eqs. (47), (61), and (70)). With the possible exception of the relatively heavy ballistic vehicle (see ref. 3) all of the hypervelocity vehicles treated here do expend the major part of their kinetic energy in flight. It is, in fact, only by virtue of this expenditure of energy that the skip and glide vehicles achieve long range. From the standpoint, then, of reducing the total heat transferred by convection, the problem is to determine how the ratio of friction force to total drag force can be reduced. This matter was discussed in detail in reference 3 in connection with ballistic vehicles and it was demonstrated that the ratio could be reduced by employing high-pressure-drag (i.e., blunt) shapes. It would be most fortunate if this avenue of solution

⁸A value of $I_e = 225$ seconds was chosen on the basis of specific impulses given for a cross section of rocket fuels in reference 4. In particular, I_e is the average I for these fuels, reduced by about 15 percent to account for staging, etc., (see eq. (3)).

were open also to the skip and glide vehicles; however, it is readily apparent that such is not the case. This conclusion follows simply from the fact that the skip and glide vehicles must develop reasonably high lift-drag ratios to achieve long range. But, as is well known, high lift-drag ratios and high pressure drag are incompatible aerodynamic properties. Evidently, then, the skip and glide vehicles will be relatively slender and they will, by comparison to blunt ballistic vehicles, be required to absorb large amounts of their kinetic energy of flight in the form of heat. On the basis of the calculations of reference 3, it does not seem feasible for slender hypervelocity vehicles to absorb and retain so much heat (of the order of one-tenth the kinetic energy of flight). We are led, therefore, to consider the possibility of radiating part or all of this heat back to the atmosphere.

Let us first consider radiation heat transfer from the surface of a glide vehicle. For purposes of simplicity we presume a vehicle conical in shape. The base diameter is taken as 3 feet and the weight as 5,000 pounds. We consider two slender cones which, according to hypersonic theory including friction drag, can develop maximum lift-drag ratios of 4 and 6 (see Appendix C). We find (see Appendix D) that the $L/D = 4$ glide vehicle can radiate heat like a black body at a rate equal to the maximum average convective heat-transfer rate if the surface temperature is allowed to rise to about 1500°F . If the vehicle develops a lift-drag ratio of 6, then the allowable surface temperature must be increased to about 1800°F . These surface temperatures are high; nevertheless they are within the range of useful strengths of available alloys. Furthermore, they can, if necessary, be reduced somewhat by designing a less dense vehicle (or, more specifically, a vehicle of lower mg/S , see Appendix D).

It is indicated, then, that the glide vehicle has the attractive possibility of radiating back to the atmosphere a large fraction of the heat transferred to it by convection.⁹ As a result the mass of coolant required to protect the vehicle may be greatly reduced. Just as with the ballistic vehicle, however (see ref. 3), it is evident that additional means, such as transpiration cooling, may well be necessary to protect local hot spots on the surface, like the stagnation region of the nose. It is also well to note that the alleviating effects of radiative cooling are not limited to the glide vehicle alone, but would apply to any hypervelocity vehicle in level flight.

We inquire now if the skip vehicle is capable of radiating heat at a rate comparable to the maximum convective heat-transfer rate. For this purpose it suffices to confine our attention to the first skip wherein the maximum convective heat-transfer rates are encountered (see eq. (64)). On the basis of our calculations for glide vehicles developing lift-drag

⁹The possibility of radiating relatively large quantities of heat from glide vehicles has, of course, been considered by others in connection with particular designs.

ratios of 4 and 6, we conclude that the skip vehicle developing comparable lift-drag ratios cannot radiate heat at anything like the maximum convective rate. This conclusion follows directly from the fact that, although the heat absorbed by the skip vehicle in the first skip would be about the same as that for the glide vehicle experiencing the same loss of kinetic energy, the rates of absorption would be far greater for the skip vehicle. Hence, the surface temperatures required for radiation to offset convection would probably exceed the temperatures at which known materials retain appreciable strength.¹⁰

Now the skip vehicle operating at lift-drag ratios in the neighborhood of 2 will absorb less heat than skip vehicles developing higher lift-drag ratios. However, as shown in Appendix D, the former vehicle still absorbs more heat than a comparable high-pressure-drag ballistic vehicle and it accrues no appreciable advantage by radiation. From the standpoint of heat transfer, then, it is indicated that the skip vehicle is inferior to both the ballistic and glide vehicles. That is to say, proportionately more coolant of one form or another would be required to protect the skip vehicle than would be required to protect ballistic or glide vehicles of the same range. The skip vehicle has other disadvantages as well. Certainly one of the most serious of these is the very high lateral loads (see fig. 3) that the vehicle would be required to withstand during a skip from the earth's atmosphere. These loads, coupled with simultaneous high thermal stresses (due to high convective rates), would require the structure to be stronger and, consequently, heavier than that of a comparable glide vehicle.¹¹ For these and other reasons concerned with problems of stability, control, and guidance, the skip vehicle is thought to be the least promising of the three types of hypervelocity vehicle considered here.

In essence, then, the preceding study has indicated that the ballistic vehicle exhibits the possibility of being relatively efficient for hypervelocity flight by virtue of the fact that aerodynamic heating can be markedly reduced through the artifice of using blunt, high-pressure-drag re-entry shapes. The disadvantage of using the relatively inefficient ballistic trajectory is counterbalanced by this advantage which tends to keep initial mass down by reducing coolant mass. The glide vehicle appears promising for hypervelocity flight because it has, coupled with the relatively high efficiency of the glide trajectory, the possibility of radiating a large fraction of the heat absorbed by convection.

¹⁰It is interesting to note, as shown in Appendix D, that a more-or-less typical vehicle, operating at a reasonable surface temperature, cannot radiate in the second ballistic phase of flight all the heat convected to it in the first skipping phase.

¹¹Added weight means, of course, added coolant (see, again, eq. (61)) which, in turn, means added weight. The performance efficiency of vehicles is reduced accordingly - indeed one can easily demonstrate that ultimately the coolant is being added to cool coolant. This situation must obviously be avoided.

Up to this point we have considered the performance efficiency of the several types of hypervelocity vehicle by comparison with each other. It is of interest now to compare, insofar as is possible, the efficiency of flight of these vehicles with that of lower speed, more conventional type aircraft.

Comparison of Hypervelocity Vehicles With the Supersonic Airplane

In the analysis of powered flight it was found that the basic performance equation for hypervelocity vehicles could be written in a form analogous to the Breguet range equation. Thus, according to equations (7) and (9), we have for both hypervelocity and lower speed vehicles that

$$R = \left(\frac{L}{D}\right)_e I_e V_e \ln \left(\frac{m_i}{m_f}\right) \quad (84)$$

where it is understood that the effective quantities are the same as the actual quantities in the case of the lower speed, more conventional aircraft. Now let us consider the product $(L/D)_e I_e V_e$. Taking first the supersonic airplane we assume flight at a Mach number of 2 and a maximum lift-drag ratio of 5. According to Schamberg (ref. 4) the product $I_e V_e$, whether the power plant be ram-jet or turbojet, is not likely to exceed about 4.4×10^6 feet.¹² The product $(L/D)_e I_e V_e$ is then 22×10^6 feet for the airplane. Now let us compare these quantities with the corresponding quantities for a ballistic vehicle and let us presume that the range will be half the circumference of the earth. In this event, the effective lift-drag ratio for the ballistic vehicle is 2π (see fig. 2) which is slightly greater than that for the airplane, while the effective velocity is just half the satellite velocity, or 13,000 feet per second. Let us again assume that the effective specific impulse is 225 seconds. In this case, the product of $I_e V_e$ is 2.9×10^6 feet which is about two thirds of that for the airplane. The product $(L/D)_e I_e V_e$ is about 18×10^6 feet which is less than, but certainly comparable to, that for the supersonic airplane. Thus we have our first suggestion that the hypervelocity vehicle is not necessarily an inefficient type vehicle for long-range flight.

In order to pursue this point further, a performance efficiency factor (see eq. (10)) defined as

$$E = \left(\frac{L}{D}\right)_e \bar{V}_e \frac{g I_e}{V_s} = \frac{\phi}{\ln \left(\frac{m_i}{m_f}\right)} \quad (85)$$

¹²This observation holds essentially for any air-breathing engine - note that the maximum value of $I_e V_e$ is simply the product of the thermal efficiency (taken as 0.3) and the specific heat content of the fuel (taken as 14.6×10^6 feet for gasoline-type fuels).

has been calculated for ballistic and glide vehicles for $I_e = 225$ seconds, and ranges up to the circumference of the earth. The corresponding quantity E has been calculated for the supersonic airplane ($I_e V_e = 4.4 \times 10^6$ feet) for several lift-drag ratios. The results of these calculations are presented in figure 10 and we observe, as our example calculation suggested, that both the ballistic and glide vehicles compare favorably with the supersonic airplane for ranges in the neighborhood of and greater than half the circumference of the earth. The glide vehicle is again superior to the ballistic vehicle at lift-drag ratios in excess of 2 and, as a result, it compares favorably with the airplane at shorter ranges than the ballistic vehicle.¹³

CONCLUDING REMARKS AND SOME DESIGN CONSIDERATIONS FOR GLIDE VEHICLES

During the course of this study it has been indicated that ballistic and glide vehicles can be operated at hypervelocities with the reasonable assurance that problems of aerodynamic heating can be largely alleviated by proper design. Skip vehicles appeared substantially less promising in this as well as other respects. It was further demonstrated that on the basis of equal ratios of initial to final mass, the long-range hypervelocity vehicle compares favorably with the supersonic airplane. These considerations suggest that the ballistic and glide vehicles have, in addition to the advantages usually ascribed to great speed, the attractive possibility of providing relatively efficient long-range flight.

In view of these findings, it seems appropriate as a final point to touch on what appear to be favorable design features of glide-type vehicles. Comparable aspects of the ballistic vehicle are not treated here inasmuch as they have already been considered in some detail in reference 3. Two categories of glide vehicle will be considered. The first category is made up of those vehicles whose flight through the earth's atmosphere is entirely at hypersonic speeds. More specifically, a vehicle in this category is required to be stable and controllable to the point of high-speed impact with the surface of the earth. The second category includes those vehicles which are required to have acceptable low-speed aerodynamic characteristics (perhaps to the point of landing).

Considering now the first category, we recognize that while the shape of the vehicle must be such as to provide reasonably high lift-drag

¹³It should be kept in mind, of course, that m_f may be substantially greater than m_p , the mass of the pay load. This point takes on particular significance with regard to expendable vehicles where m_i/m_p is perhaps a better measure of cost than m_i/m_f . Thus, noting that $m_i/m_p = (m_i/m_f)(m_f/m_p)$, and recognizing that m_f/m_p is probably lowest for the ballistic vehicle, we anticipate that the ballistic vehicle would appear to better advantage than shown in figure 10.

ratios, it should also be a compact configuration designed to minimize structural and, hence, propellant weight. Furthermore, it appears most desirable from the standpoint of aerodynamic heating to eliminate all surfaces that present extremely severe heating problems. These considerations tend naturally to focus our attention on configurations free of the planar surfaces normally used for developing lift and providing stable and controlled flight. We pursue this point, therefore, by inquiring of the efficiency of a body of revolution as a lifting device at hypersonic speeds. For this purpose, theory, including friction drag estimates, was employed to calculate the maximum lift-drag ratios of cones and flat plates (see Appendix E) and the results are presented in figure 11. It is seen that while the flat plate is, as would be expected, by far the most efficient lifting device at low supersonic speeds ($1/M \rightarrow 1$), it has but little advantage over the cone at hypersonic speeds ($1/M \rightarrow 0$).¹⁴ Evidently, then, the body of revolution is relatively efficient for developing lift at hypersonic speeds.

Now, it is clear (see eq. (78)) that just as with the ballistic vehicle, the nose of the glide vehicle should be rounded to alleviate the local heating problem. There is evidence, both theoretical and experimental that in addition to alleviating the heating problem, rounding the nose may, in fact, increase the lifting efficiency of a body. Recalling that for slender bodies the maximum lift-drag ratio is governed primarily by zero-lift drag, we recognize the validity of this statement on the basis of the theoretical and experimental work of reference 9 and the experimental work of reference 10.

The body must, of course, be stable and controllable in flight. Recent experimental work in reference 11 indicates that these requirements may be satisfied without recourse to planar surfaces. Stability in pitch and yaw is provided by a conical flare at the base of the body, and control in pitch and yaw is provided by deflectable sections of the surface of the body. These sections are located on the rear portion of the body to provide a configuration which is inherently stable in roll. A hypervelocity glide vehicle in the first category might, then, in view of these considerations, appear something like that shown in figure 12 which is repeated from reference 11.

Consider now a glide vehicle falling in category two. First of all, it appears most unlikely that acceptable low-speed aerodynamic characteristics can be obtained without using more conventional planar surfaces, at least to the extent of a wing. The question then is: What can be done to alleviate the aerodynamic heating of planar surfaces? Especially in this regard are we concerned with the very severe heating encountered

¹⁴This conclusion is not to be construed as contradicting the findings of Resnikoff, reference 8, which presumed an inviscid hypersonic flow. Certainly too, as demonstrated experimentally by Resnikoff, the low-aspect-ratio wedge wing will generally be superior to the body of revolution in the speed range of his tests ($M = 5$).

at the leading edges of these surfaces. It is apparent by analogy to the nose of the body that the severity of aerodynamic heating at the leading edge of a wing can be reduced by simply rounding the leading edge. In fact, on comparing the theoretical results of references 12 and 13, we see that for the purposes of this report there is no essential difference between the heat-transfer rate at the stagnation point of a blunt leading edge and that at the stagnation point of a comparable blunt nose as given by equation (44). We may anticipate, however, that rounding the leading edge will incur a drag penalty which will, in turn, reduce the attainable lift-drag ratios. This difficulty may be largely circumvented by simply sweeping the leading edge of the wing. The contribution to total drag of the drag at the leading edge is in this manner reduced approximately in proportion to the square of the cosine of the angle of sweep. Equally important, the rate of heat transfer to the leading edge may also be substantially decreased by sweep. This possibility is suggested by the independence principle for cylindrical viscous flows (refs. 14 and 15) which applies to the components of flow normal and parallel to the axis of a cylinder.¹⁵ We conclude, therefore, that in the event rounded leading edges are used to alleviate heat transfer to wings of glide vehicles, or for that matter any hypersonic vehicle, these wings might well have highly swept leading edges. One is lead naturally to consider triangular or delta plan form configurations. By entirely analogous reasoning, the triangular plan form may also prove desirable for stabilizing and controlling surfaces.

It is entirely possible, of course, and perhaps even desirable, that wing-body junctures of a glide vehicle should not be discontinuous but rather that the body, in effect, should be simply flattened out to appear more or less elliptic in cross section. In any event we see that, interestingly enough, the concept of sweepback may play an important role in reducing the heating and drag of practical configurations at hypersonic speeds, much as it has for drag alone at supersonic speeds.

Ames Aeronautical Laboratory
National Advisory Committee for Aeronautics
Moffett Field, Calif., Dec. 10, 1954

¹⁵According to the independence principle and equation (44), heat-transfer rates will be reduced by the cube of the cosine of the leading-edge sweep angle. This principle is, of course, not strictly applicable to viscous flow about blunt cylinders. Actually, there may be a sizable contribution to heat transfer by the component of flow parallel to the leading edge, and unpublished theoretical and experimental results indicate that the reduction in heat transfer may be more nearly proportional to the square of the cosine of the sweep angle. In any case, it is sufficient for the purposes of this report, to note that a sizable reduction in heat transfer is achieved by sweeping a blunt leading edge.

APPENDIX A

NOTATION

A	reference area for lift and drag evaluation, sq ft
C	specific heat of vehicle material, ft-lb/slug $^{\circ}\text{R}$
C_D	drag coefficient
C_L	lift coefficient
C_F	skin-friction coefficient
C_F'	equivalent skin-friction coefficient, (see eq. (40))
C_p	specific heat of air at constant pressure ft-lb/slug $^{\circ}\text{R}$
C_v	specific heat of air at constant volume, ft-lb/slug $^{\circ}\text{R}$
D	drag, lb
e	Naperian logarithm base
E	performance efficiency factor, (see eq. (85))
f	general functional designation
F_a, F_b	functions of ΔJ , (see eqs. (74) and (80))
g	acceleration due to force of gravity, ft/sec ²
h	convective heat-transfer coefficient, ft-lb/ft ² sec $^{\circ}\text{R}$
H	convective heat transferred per unit area (unless otherwise designated), ft-lb/ft ²
I	specific impulse, sec
J	range parameter for glide vehicle (see eq. (68))
k	Stefan-Boltzman constant for black body radiation (3.7 $\times 10^{-10}$ ft-lb/ft ² sec $^{\circ}\text{R}^4$)
L	lift, lb
m	mass, slugs
M	Mach number

Q	convective heat transferred (unless otherwise designated), ft-lb
r	distance from center of the earth, ft
r_c	radius of curvature of flight path, ft
r_o	radius of earth, ft
R	range, ft
s	distance along flight path, ft
S	surface area, sq ft
t	time, sec
T	temperature (ambient air temperature unless otherwise specified), $^{\circ}\text{R}$
V	velocity, ft/sec
\bar{V}	ratio of velocity to satellite velocity
V_S	velocity of satellite at earth's surface (taken as 25,930 ft/sec)
W	weight, lb
y	vertical distance from surface of earth, ft
α	angle of attack, radians unless otherwise specified
β	constant in density-altitude relation, $(22,000 \text{ ft})^{-1}$
γ	ratio of specific heats, C_p/C_v
δ	semivertex angle of cones, radians unless otherwise specified
Δ	increment
η	lift-drag efficiency factor, (see eq. (C27))
θ	angle of flight path to horizontal, radians unless otherwise specified
λ	function of Mach number, (see eq. (E7))
ρ	air density, slugs/cu ft ($\rho_o = 0.0034$)

σ	nose or leading-edge radius of body or wing, ft
ϕ	partial range, radians
Φ	total range, radians
ψ	remaining range ($\Phi - \phi$), radians

Subscripts

o	conditions at zero angle of attack
1,2,3,...	conditions at end of particular rocket stages
a	conditions at point of maximum average heat-transfer rate
av	average values
b	conditions at point of maximum local heat-transfer rate
C	convection
e	effective values
en	conditions at entrance to earth's atmosphere
ex	conditions at exit from earth's atmosphere
f	conditions at end of powered flight
i	initial conditions
l	local conditions
n	ballistic phases of skip vehicles
N	total number of rocket stages
p	pressure effects
P	pay load
r	recovery conditions
R	radiation
s	stagnation conditions
T	total values
w	wall conditions

APPENDIX B

SIMPLIFYING ASSUMPTIONS IN THE ANALYSIS OF THE GLIDE TRAJECTORY

The assumption of small deflection angle ($\theta \ll 1$) was used throughout the study of the glide trajectory. In addition, equation (28) was simplified on the assumptions that

$$(L/D)\theta \ll 1 \quad (B1)$$

and

$$V^2 \frac{d\theta}{ds} \ll \frac{L/D}{2} \frac{dV^2}{ds} \quad (B2)$$

The extent to which these assumptions are permissible can be checked by deriving an expression for $(L/D)\theta$ and examining its variation over a range of trajectory parameters.

From equations (30), (33), and (34) the altitude of any point in a glide trajectory is found to be

$$y = \frac{1}{\beta} \left\{ \ln \left[\frac{1 - (1 - \bar{V}_f^2)e^J}{(1 - \bar{V}_f^2)e^J} \right] + \ln \left(\frac{1 - \bar{V}_{r=r_0}^2}{\bar{V}_{r=r_0}^2} \right) \right\} \quad (B3)$$

By retaining the assumption of small inclination angle, whereby $\theta \approx -dy/ds$, and recalling that $J = (2s/r_0)/(L/D)$, we find the inclination angle by differentiating equation (B3). Performing this operation and making use of equation (30) reduces the expression for $(L/D)\theta$ to

$$\frac{L}{D} \theta = \frac{2}{\beta r_0} \left[\frac{1}{1 - (1 - \bar{V}_f^2)e^J} \right] = \frac{2.105 \times 10^{-3}}{\bar{V}^2} \quad (B4)$$

Since \bar{V}^2 becomes very small toward the end of the trajectory, it is apparent from equation (B4) that the assumption of small $(L/D)\theta$ cannot be justified in this portion of flight. The problem then is to determine the conditions under which $(L/D)\theta$ remains negligibly small over the major part of the trajectory.

With the aid of equations (30) and (36), equation (B4) can be modified to the following form

$$\frac{\phi}{\Phi} = 1 - \frac{L/D}{\Phi} \ln \left\{ \frac{1}{1 - \left[\frac{2/\beta r_0}{(L/D)\theta} \right]} \right\} \quad (B5)$$

For given values of L/D and total range Φ , equation (B5) determines the fractional part of the total range which corresponds to a given value of $(L/D)\theta$. Since the deflection angle is always increasing, we can therefore determine the portion of the total range through which $(L/D)\theta$ remains equal to or less than a given value. A computation of this nature was performed for a value of $(L/D)\theta \leq 0.05$, and the results are presented in figure 13. From this figure we can see that except for short ranges and large lift-drag ratios, $(L/D)\theta$ (as well as θ) remains at a value less than 0.05 for better than 90 percent of the total range.

The second assumption, equation (B2), can also be verified from the results of the analysis. By differentiation of equation (B4) we find that

$$v^2 \frac{d\theta}{ds} = \frac{4V_s^2}{\beta r_0^2 (L/D)^2} \left[\frac{(1 - \bar{V}_f^2) e^J}{\bar{V}^2} \right] \quad (B6)$$

while differentiation of equation (30) yields

$$\frac{1}{2} (L/D) \frac{dV^2}{ds} = - \frac{V_s^2 (1 - \bar{V}_f^2) e^J}{r_0} \quad (B7)$$

Dividing equation (B6) by equation (B7), and making use of equation (B4), we find that

$$\frac{v^2 \frac{d\theta}{ds}}{\frac{1}{2} (L/D) \frac{dV^2}{ds}} = \frac{2\theta}{(L/D)} = \frac{2}{(L/D)^2} [(L/D)\theta] \quad (B8)$$

By comparing equation (B8) with the previous results obtained for $(L/D)\theta$, (fig. 13) we can readily see that this assumption, equation (B2), is actually less stringent than the previous one for practical values of L/D .

APPENDIX C

THE RELATION BETWEEN $\frac{C_F'S}{C_D A}$ AND $\left(\frac{L}{D}\right)_{\max}$ FOR CONICAL MISSILES

The lift and drag coefficients for slender cones at small angles of attack can be expressed in the following manner:

$$C_L = 2\alpha \quad (C1)$$

$$C_D = C_{D_0} + \alpha C_L \quad (C2)$$

By dividing the first of the preceding equations by the second, one can obtain an expression for the lift-drag ratio

$$\frac{L}{D} = \frac{C_L}{C_D} = \frac{C_L}{C_{D_0} + \alpha C_L} = \frac{C_L}{C_{D_0} + C_L^2/2} \quad (C3)$$

It can be shown that equation (C3) has a maximum value when

$$C_{D_0} = C_L^2/2 \quad (C4)$$

whereby

$$(C_D)_{(L/D)_{\max}} = 2C_{D_0} \quad (C5)$$

From equations (C1) through (C5), the maximum value of the lift-drag ratio can be expressed in the following ways:

$$\left(\frac{L}{D}\right)_{\max} = \frac{1}{2\alpha} = \frac{1}{C_L} = \frac{1}{\sqrt{2C_{D_0}}} \quad (C6)$$

The drag coefficient at zero angle of attack appearing in equation (C2) can be broken down into its component parts to yield

$$C_{D_0} = (C_{D_0})_p + C_{F_0} S/A \quad (C7)$$

where $(C_{D_o})_p$ is the zero-lift pressure drag coefficient and C_{F_o} is the zero-lift skin-friction coefficient based on wetted area. The skin-friction coefficient, C_{F_o} , in equation (C7) can be related to the equivalent skin-friction, $C_{F'}$, (see eq. (43)) by considering average conditions over the surface of the cone. Equating the friction drags as determined from free-stream and local average conditions, it is found that

$$C_{F_o} = (C_{F_l})_{av} \frac{(\rho_l)_{av}(V_l)_{av}^2}{\rho V^2} \quad (C8)$$

By referring to local average conditions on the body surface, the expression for $C_{F'}$, equation (40), can be written as

$$C_{F'} = (C_{F_l})_{av} \frac{(\rho_l)_{av}(V_l)_{av}}{\rho V} \quad (C9)$$

Comparing equations (C8) and (C9) it is apparent that

$$C_{F_o} = C_{F'} \frac{(V_l)_{av}}{V} \quad (C10)$$

For slender shapes at hypersonic speeds, the local velocity does not differ appreciably from the free-stream value. Also, for small angles of attack, the skin-friction coefficient should remain fairly constant. Consequently, equation (C10) can be written as

$$C_{F_o} = C_F = C_{F'} = \text{constant} \quad (C11)$$

and equation (C7) then becomes

$$C_{D_o} = (C_{D_o})_p + \frac{C_{F'} S}{A} \quad (C12)$$

From equations (C5) and (C12) it can then be shown that

$$\left(\frac{C_{F'} S}{C_D A} \right)_{(L/D)_{max}} = \frac{1}{2} \left[1 - \frac{(C_{D_o})_p}{C_{D_o}} \right] \quad (C13)$$

From the Newtonian impact theory, the zero-lift pressure drag coefficient for slender cones at hypersonic speeds can be expressed as

$$(C_{D_o})_p = 2\delta^2 \quad (C14)$$

where δ is the semivertex angle of the cone. By further noting that for slender cones

$$\frac{S}{A} = \frac{1}{\delta} \quad (C15)$$

equation (C12) then becomes

$$C_{D_o} = 2\delta^2 + \frac{C_{F'}}{\delta} \quad (C16)$$

For a given value of $C_{F'}$ it can be shown that equation (C16) has minimum value when

$$\delta = \delta_{opt} = \left(\frac{C_{F'}}{4} \right)^{1/3} \quad (C17)$$

whereby, at $\delta = \delta_{opt}$

$$(C_{D_o})_{min} = 6\delta_{opt}^2 = 3(C_{D_o})_p \quad (C18)$$

Obviously, then, the highest value of maximum lift-drag ratio (eq. (C6)) will be attained by the cone with the semivertex angle given by equation (C17). By substitution from equation (C18) into equation (C6), the optimum value of maximum lift-drag ratio is

$$\left(\frac{L}{D} \right)_{max} = \frac{1}{2\sqrt{3}} \left(\frac{4}{C_{F'}} \right)^{1/3} = \frac{1}{2\sqrt{3} \delta_{opt}} \quad (C19)$$

By further substituting the expression for minimum zero-lift drag coefficient, equation (C18), into equation (C13), the following relation, corresponding to the condition of optimum maximum lift-drag ratio, is obtained:

$$\left(\frac{C_{F'} S}{C_{DA}} \right)_{(L/D)_{max}} = \frac{1}{3} \quad (C20)$$

With the aid of equations (C14) and (C16), equation (C13) can also be expressed in the following form, corresponding to any maximum lift-drag ratio including the optimum value:

$$\left(\frac{C_F'S}{C_{DA}}\right)_{(L/D)_{\max}} = \frac{1}{2} \left(1 - \frac{1}{1 + \frac{C_F'}{2\delta^3}}\right) \quad (C21)$$

From equations (C20) and (C21) it can readily be seen that in the case of the optimum $(L/D)_{\max}$

$$\frac{C_F'}{2\delta_{\text{opt}}^3} = 2 \quad (C22)$$

from which it follows directly that

$$\frac{C_F'}{2\delta^3} = 2 \left(\frac{\delta_{\text{opt}}}{\delta}\right)^3 \quad (C23)$$

so that equation (C21) may be written as

$$\left(\frac{C_F'S}{C_{DA}}\right)_{(L/D)_{\max}} = \frac{1}{2 + \left(\frac{\delta}{\delta_{\text{opt}}}\right)^3} \quad (C24)$$

With the aid of equations (C16) and (C23), the expression for any $(L/D)_{\max}$ (eq. (C6)) can be shown to be

$$\left(\frac{L}{D}\right)_{\max} = \frac{1}{2\delta \left[1 + 2 \left(\frac{\delta_{\text{opt}}}{\delta}\right)^3\right]^{1/2}} \quad (C25)$$

and it follows directly from equation (C19) that the ratio of $(L/D)_{\max}$ for any cone to that for the optimum cone is

$$\eta = \frac{\delta_{\text{opt}}}{\delta} \left[\frac{3}{1 + 2 \left(\frac{\delta_{\text{opt}}}{\delta} \right)^3} \right]^{1/2} \quad (C26)$$

where η is defined as the "lift-drag efficiency factor." By substitution from equation (C24), the ratio of $(L/D)_{\text{max}}$ to the optimum value can then be expressed in terms of $(C_F'S/C_{DA})$ as follows:

$$\eta = \sqrt{3} \left(\frac{C_F'S}{C_{DA}} \right)^{1/3} \left(1 - 2 \frac{C_F'S}{C_{DA}} \right)^{1/6} \quad (C27)$$

The dependence of η on $C_F'S/C_{DA}$ is shown in figure 14. It should be noted, however, that for small values of η the assumption of slender cones will be violated, although the results as shown will be qualitatively correct in that $C_F'S/C_{DA}$ will become exceedingly small for low values of $(L/D)_{\text{max}}$ regardless of body shape.

APPENDIX D

COMPUTATION OF HEATING ASSOCIATED WITH ROCKET VEHICLES

Radiation of Heat From Glide Vehicles

From equation (72), the maximum time rate of total heat input to the glide vehicle can be expressed as

$$\left(\frac{dQ}{dt}\right)_{\max} = S \left(\frac{dH_{av}}{dt}\right)_{\max} = \frac{mgVs}{3\sqrt{3}(L/D)} \left(\frac{C_F'S}{C_{DA}}\right) \quad (D1)$$

The rate of heat radiation from the vehicle can be expressed by the following standard relation

$$S \frac{dH_R}{dt} = kT^4S \quad (D2)$$

Using equations (D1) and (D2), the requirement for continuous radiation of all convective heat input to a surface at a temperature 2000°R (1540°F) can be expressed as

$$\frac{mg}{S(L/D)} \frac{C_F'S}{C_{DA}} \leq 1.20 \quad (D3)$$

If a value of $(L/D)_{\max}^{\text{opt}} = 6$ is assumed, values of the parameter $C_F'S/C_{DA}$ and cone angle, δ , can be determined as a function of actual $(L/D)_{\max}$ from the analysis given in Appendix C. A vehicle weight of 5000 pounds with a maximum diameter of 3 feet is assumed whereby equation (D3) can be evaluated for various (L/D) giving the results in the following table:

L/D	$C_F'S/C_{DA}$	δ , deg	S, sq ft	$\frac{mg}{S(L/D)} \frac{C_F'S}{C_{DA}}$
6	0.333	2.75	147	1.89
4	.0600	6.73	60.2	1.24
2	.00710	14.3	28.6	.619
1	.000890	29.6	14.3	.312
1/2	.000115	55.8	8.55	.135

We see, therefore, that at surface temperatures of 2000° R and for an L/D of 4, this glide-type vehicle can radiate heat at a rate equal to or greater than the maximum convective heat rate.

Radiative and Convective Heat Transfer Associated With Skip Vehicle

In this section the problem is to determine the extent to which heat absorbed by a skip vehicle in the first skipping phase, can be reradiated during the subsequent ballistic phase. The quantity of heat absorbed in the first skipping phase has already been obtained in the heating analysis, (eq. (59) for $n = 1$)

$$\frac{Q_1}{\frac{1}{2} m V_f^2} = \frac{1}{2} \frac{C_F' S}{C_{DA}} \left(1 - e^{-\frac{4\theta_f}{L/D}} \right) \quad (D4)$$

where the total heat absorbed throughout the entire trajectory is

$$\frac{Q_T}{\frac{1}{2} m V_f^2} = \frac{1}{2} \frac{C_F' S}{C_{DA}} \quad (D5)$$

In order to determine the heat radiated, three quantities must be determined:

1. Temperature of the vehicle at the start of the second ballistic phase
2. Temperature of the vehicle at the end of the second ballistic phase
3. The time duration of the second ballistic phase

To determine the first of the above quantities, we employ the relation for heat absorbed

$$Q_1 = c W_e \Delta T \quad (D6)$$

where c is the specific heat of the material, W_e is the effective weight of material absorbing heat, and ΔT is the temperature rise during the first skip. If it is assumed that $1/3$ of the missile weight will

absorb heat, equation (D6) becomes

$$\Delta T = \frac{3}{gc} \left(\frac{Q_1}{m} \right) \quad (D7)$$

where m is the total mass of the vehicle. It is assumed that the material has a specific heat of 0.11 Btu/lb °R. If it is also assumed that the temperature at the start of the first skip is 500° R, equation (D7) becomes

$$T_{ex2} = 500 + 1.1 \times 10^{-3} \left(\frac{Q_1}{m} \right) \quad (D8)$$

which defines the temperature at the beginning of the second ballistic phase.

To find the temperature at the end of the second ballistic phase, we equate the radiant heat-transfer rate from the body to the rate of heat loss in terms of the temperature drop of the body

$$-kT^4 S dt = cW_e dT \quad (D9)$$

This expression can be integrated between limits from beginning to end of the second ballistic phase to yield

$$T_{en2}^3 = \frac{1}{(7.95 \times 10^{-15}) S t + \frac{1}{T_{ex2}}} \quad (D10)$$

for a vehicle weight of 5000 pounds (effective absorbing weight of 1667 pounds) where T_{en2} is the temperature at the end of the second ballistic phase and t is the total time of the second ballistic phase. The total heat lost by radiation can now be expressed in terms of the temperature drop as

$$Q_{R2} = (T_{ex2} - T_{en2}) W_e c$$

or

$$Q_{R2} = 1.41 \times 10^5 (T_{ex2} - T_{en2}) \quad (D11)$$

From reference 7, in combination with the results presented for the motion of a ballistic vehicle (eq. (11)), the time of flight in any ballistic trajectory can be expressed as

$$t = \frac{2r_0}{V_s} \frac{\left(1 - \cos \frac{\Phi}{2}\right)^{3/2}}{(1 - i^2)} \left[\tan \theta_f + \frac{2}{\sqrt{1 - i^2}} \tan^{-1} \left(\sqrt{\frac{1 + i}{1 - i}} \tan \frac{\Phi}{4} \right) \right] \quad (D12)$$

where

$$i = \frac{\tan \theta_f}{\sin \frac{\Phi}{2} + \tan \theta_f \cos \frac{\Phi}{2}}$$

$$\frac{\Phi}{2} = \tan^{-1} \left(\frac{\sin \theta_f \cos \theta_f}{\frac{1}{\sqrt{2}} - \cos^2 \theta_f} \right)$$

The foregoing relations were applied to a computation of the radiative cooling of a missile weighing 5000 pounds and traversing a total range of 3440 nautical miles ($\Phi = 1.0$). Values of θ_f were obtained in the motion analysis, whereas values of $C_F'S/C_DA$ and S obtained in the previous calculation with regard to the glide missile will apply to this case also. The computations are summarized in the following table. Note that the case of $L/D = 1/2$ is essentially the ballistic vehicle (see fig. 9).

L/D	θ_f , deg	\bar{V}_f^2	$Q_1 \times 10^{-5}$	Q_1/Q_T	t, sec	T_{ex2} , $^{\circ}R$	T_{en2} , $^{\circ}R$	$Q_{R2} \times 10^{-5}$	Q_{R2}/Q_1
6	12.5	0.275	3115	0.135	213	2710	1490	1725	0.554
4	17.0	.315	1470	.258	335	1542	1323	316	.211
2	24.0	.525	549	.575	395	889	885	27	.049
1	27.5	.620	122	.853	247	587	585	3	.023
1/2	30.0	.650	19	.985	80.4	514	514	0	0

We see, therefore, that the quantity of heat which must be absorbed by this skip vehicle decreases rapidly with decreasing lift-drag ratio. The quantity of heat which must be absorbed by a ballistic vehicle ($L/D \approx 1/2$) is almost negligible compared with the quantities associated with vehicles with an $L/D = 2$ or greater. Comparison of the heat absorbed in the first skipping phase with the heat radiated in the second ballistic phase indicates no appreciable advantage is obtained due to radiation for

values of $L/D = 2$ and lower. To be sure, this situation could be substantially altered (near $L/D = 2$) by allowing the surface temperatures to reach higher values during the skip; however, it seems most unlikely that the net heat absorbed by the skip vehicle could ever be reduced to the low value of the ballistic vehicle for any reasonable surface temperature.

APPENDIX E

DETERMINATION OF THE RATIO OF $(L/D)_{\max}$ FOR
A FLAT PLATE TO $(L/D)_{\max}$ FOR A CONE

In Appendix C the expression for the optimum $(L/D)_{\max}$ for a slender cone was developed with the assumption of large Mach numbers and a constant value of C_F' . A simple analysis will now be presented whereby it is shown that equation (C19) will apply, for the most part, throughout the Mach number range and for a variable C_F' . Inasmuch as the lift coefficient (eq. (C1)) is essentially independent of Mach number and cone angle, modification of the results obtained in Appendix C (eq. (C19)) will occur only through the evaluation of the zero-lift drag coefficient (eq. (C6)).

The variation with Mach number of the zero-lift pressure-drag coefficient, $(C_{D_0})_p$, can be represented as

$$(C_{D_0})_p = 2f(M)\sin^2\delta \quad (E1)$$

while C_F' is assumed to vary with cone angle in the following manner

$$C_F' = C_{F'_{m=0}} \delta^m \quad (E2)$$

where m is chosen to give the required variation of C_F' with δ . By an analysis paralleling that presented in Appendix C, it can be shown that the optimum value of the lift-drag ratio assumes the following form

$$\left(\frac{L}{D}\right)_{\max} = \frac{1}{2\sqrt{3}} \left(\frac{4}{C_{F'}}\right)^{1/3} \sqrt{\frac{(1-m)^{1/3}}{(1-m/3)}} \frac{1}{[f(M)]^{1/6}} \quad (E3)$$

Now the values of $f(M)$ should not differ greatly from 1 while values of m should not differ greatly from 0. It follows then that values of $(L/D)_{\max}$ obtained from equation (E3) will not differ appreciably from those obtained from equation (C19). Furthermore, the coefficient C_F' will not differ appreciably from C_F for the slender shapes and small angles of attack under consideration. Equation (E3) then reduces to the form

$$\left(\frac{L}{D}\right)_{\max} = \frac{1}{2\sqrt{3}} \left(\frac{h}{C_F}\right)^{1/3} \quad (E4)$$

which corresponds to equation (C19) and is also a suitable approximation for all supersonic Mach numbers.

For a flat plate in supersonic flow, the lift and drag coefficients can be expressed as

$$C_L = \frac{4\alpha}{\sqrt{M^2 - 1}} + 2\alpha^2 \quad (E5)$$

$$C_D = C_{D_0} + \alpha C_L \quad (E6)$$

which follows easily from the equation for pressure coefficient given by Ivey and Cline (ref. 16). By noting that

$$C_{D_0} = 2C_F$$

the lift-drag ratio can be written from equations (E5) and (E6) as

$$\frac{L}{D} = \frac{2\lambda\alpha + \alpha^2}{C_F + 2\lambda\alpha^2 + \alpha^3} \quad (E7)$$

where

$$\lambda = \frac{1}{\sqrt{M^2 - 1}}$$

Equation (E7) is found to have the following maximum value

$$\left(\frac{L}{D}\right)_{\max} = \frac{1}{\alpha + \frac{\alpha^3}{2(\lambda + \alpha)(2\lambda + \alpha)} + \frac{2\alpha\lambda}{(2\lambda + \alpha)}} \quad (E8)$$

which occurs at values of the independent variables given by the maximum condition

$$C_F = \alpha^2 \left[2\lambda + \frac{\alpha^2}{2(\lambda + \alpha)} \right] \quad (E9)$$

From equations (E4), (E8), and (E9), and recalling that $\lambda = (M^2 - 1)^{-1/2}$ the ratio of $(L/D)_{\max}$ for a flat plate to $(L/D)_{\max}$ for a cone can be determined as a function of Mach number and C_F . The variation of this ratio with Mach number for given values of C_F has been presented in figure 11, where it was found convenient to use the inverse Mach number as the abscissa in order to illustrate conveniently the behavior at hypersonic speeds.

REFERENCES

1. Sanger, Eugen: Raketen-flugtechnik. R. Oldenbourg (Berlin), 1933.
2. Sanger, Eugen, and Bredt, J.: A Rocket Drive for Long Range Bombers. Tech. Information Branch, Navy Department, Trans. CGD-32, 1944.
3. Allen, H. Julian, and Eggers, A. J., Jr.: A Study of the Motion and Aerodynamic Heating of Missiles Entering the Earth's Atmosphere at High Supersonic Speeds. NACA RM A53D28, 1953.
4. Schamberg, R.: Effects of Flight Speed and Propulsive System on Aircraft Range. The RAND Corporation, R-114, Aug. 13, 1948.
5. Malina, Frank J., and Summerfield, Martin: The Problem of Escape from the Earth by Rocket. Jour. Aero. Sci., vol. 14, no. 8, Aug. 1947, pp. 471-480.
6. Timoshenko, S., and Young, D. H.: Advanced Dynamics. McGraw-Hill, 1948.
7. King-Hele, D. G., and Gilmore, D. M. C.: Long-Range Surface-to-Surface Rocket Missiles: Properties of Ballistic Trajectories in Vacuo. R.A.E. TN No. G. W. 305, Mar. 1954.
8. Resnikoff, Meyer M.: Optimum Lifting Bodies at High Supersonic Airspeeds. NACA RM A54B15, 1954.
9. Eggers, A. J., Jr., Dennis, David H., and Resnikoff, Meyer M.: Bodies of Revolution for Minimum Drag at High Supersonic Airspeeds. NACA RM A51K27, 1952.
10. Sommer, Simon C., and Stark, James A.: The Effect of Bluntness on the Drag of Spherical Tipped Truncated Cones of Fineness Ratio 3 at Mach Numbers 1.2 to 7.4. NACA RM A52B13, 1952.
11. Eggers, A. J., Jr., and Syvertson, Clarence A.: Experimental Investigation of a Body Flare for Obtaining Pitch Stability and a Body Flap for Obtaining Pitch Control in Hypersonic Flight. NACA RM A54J13, 1954.
12. Sibulkin, M.: Heat Transfer Near the Forward Stagnation Point of a Body of Revolution. Jour. Aero. Sci., vol. 19, no. 8, Aug. 1952, pp. 570-571.
13. Goldstein, S.: Modern Developments in Fluid Mechanics, 1st edition, vol. 2, Oxford Univ. Press, London, 1938, pp. 631-632.

14. Prandtl, L.: On Boundary Layers in Three-Dimensional Flow. M.A.P., Volkenrode (Rep. and Trans. No. 64), May 1, 1946.
15. Jones, Robert T.: Effects of Sweepback on Boundary Layer and Separation. NACA Rep. 884, 1947. (Formerly NACA TN 1402)
16. Ivey, H. Reese, and Cline, Charles W.: Effect of Heat-Capacity Lag on the Flow Through Oblique Shock Waves. NACA TN 2196, 1950.

~~CONFIDENTIAL~~

NACA RM A54L10

~~CONFIDENTIAL~~

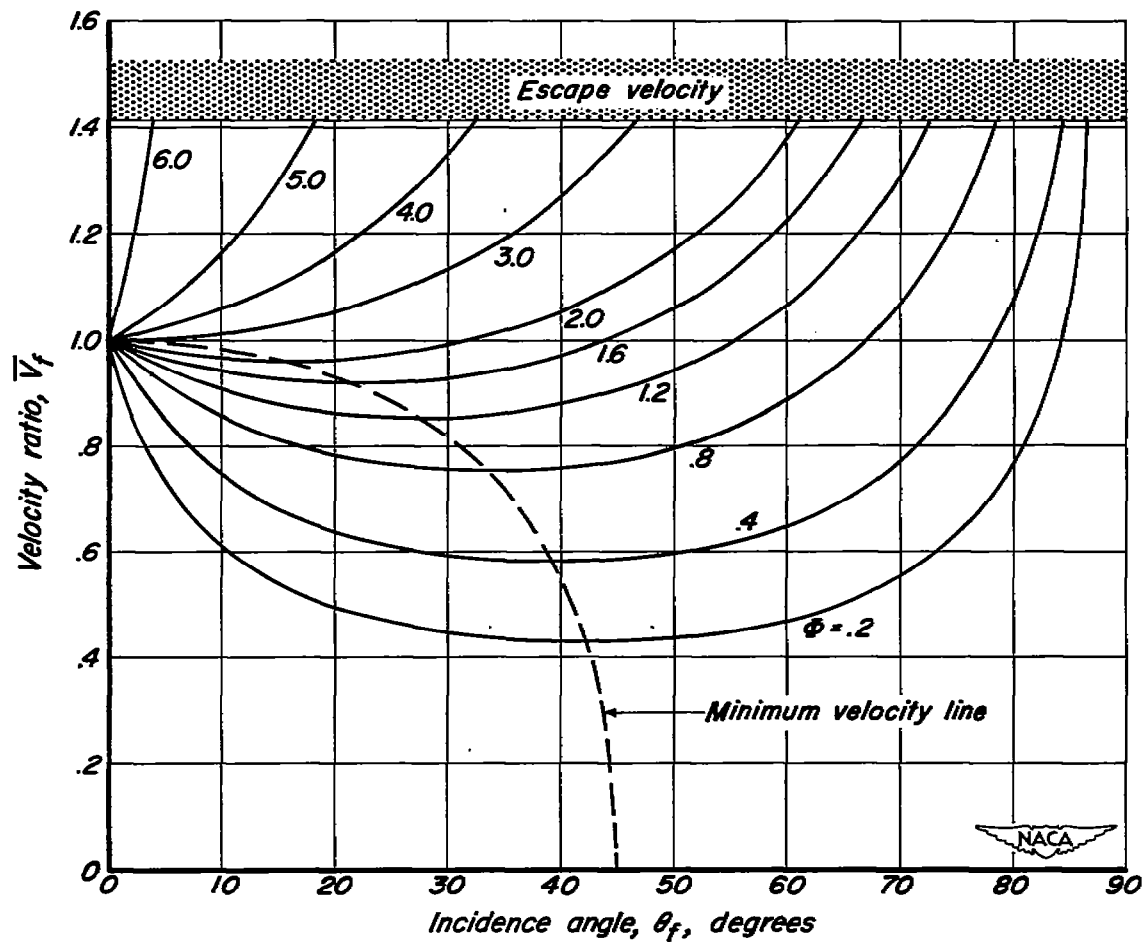


Figure 1.— Variation of velocity with incidence angle for various values of range of ballistic vehicle.

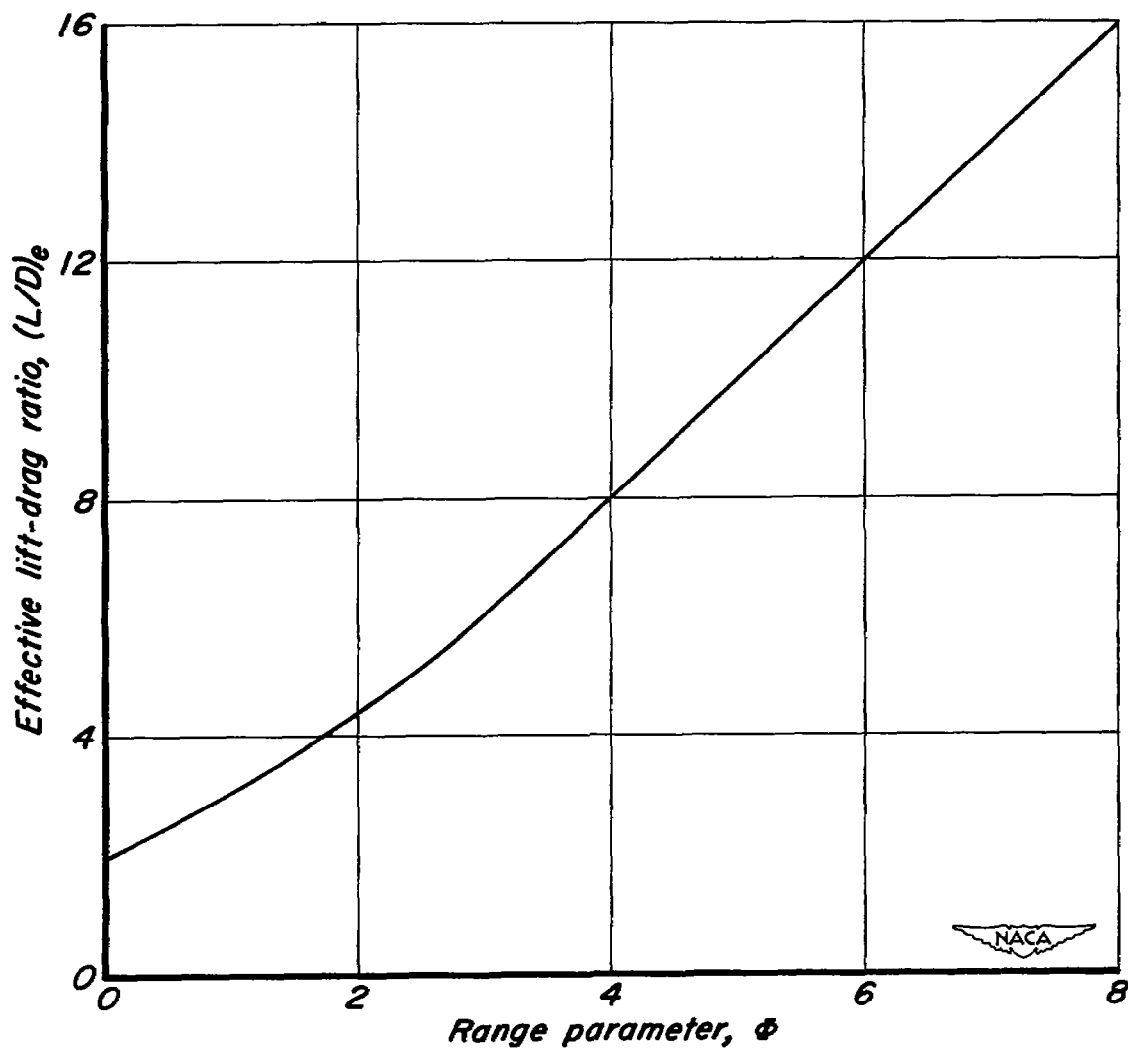


Figure 2.— Variation of effective lift-drag ratio with range for optimum ballistic vehicle.

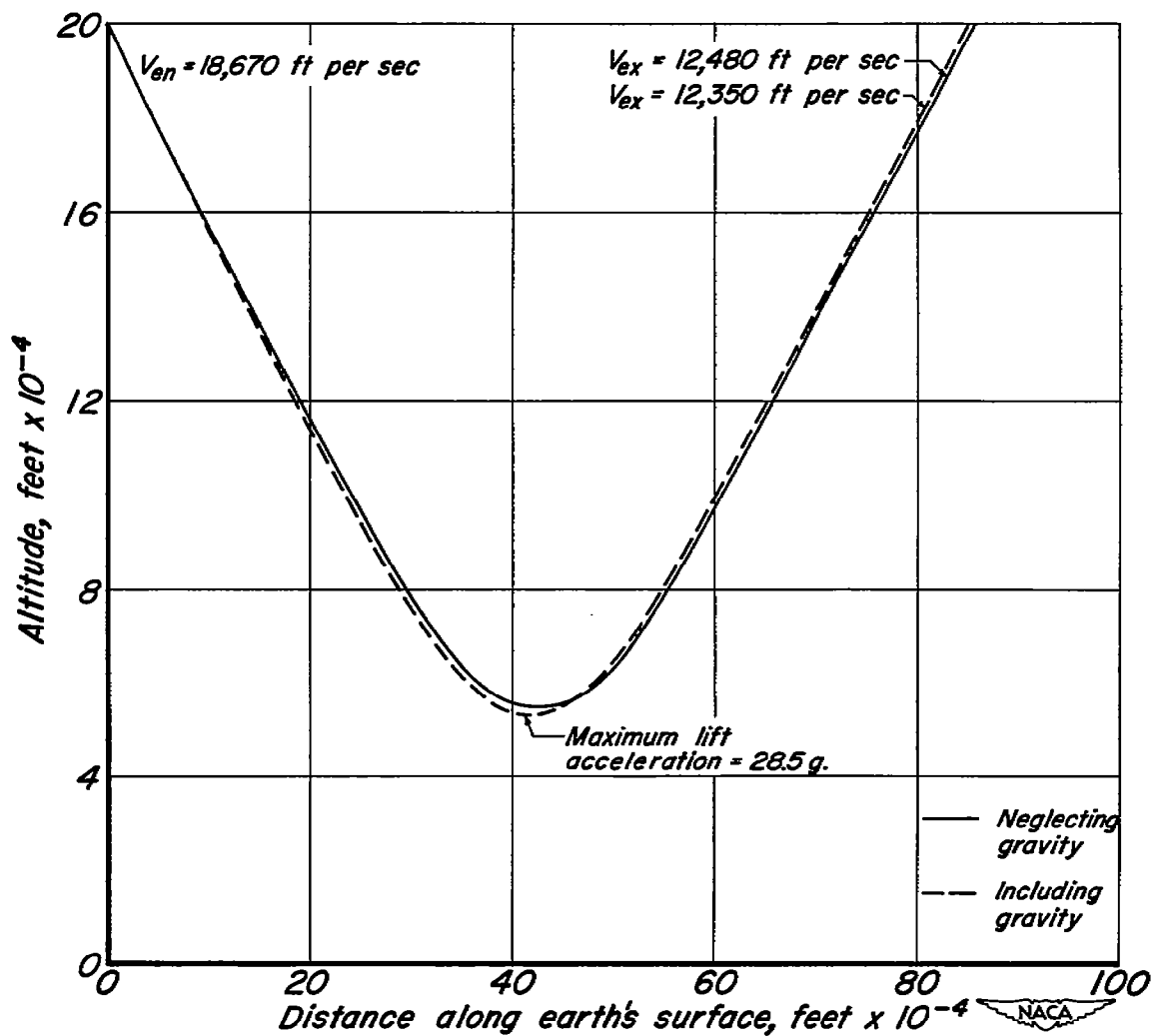


Figure 3.— Trajectory of the first skipping phase for a skip vehicle with a lift-drag ratio of 2 and a total range of 3440 nautical miles ($\Phi = 1$).

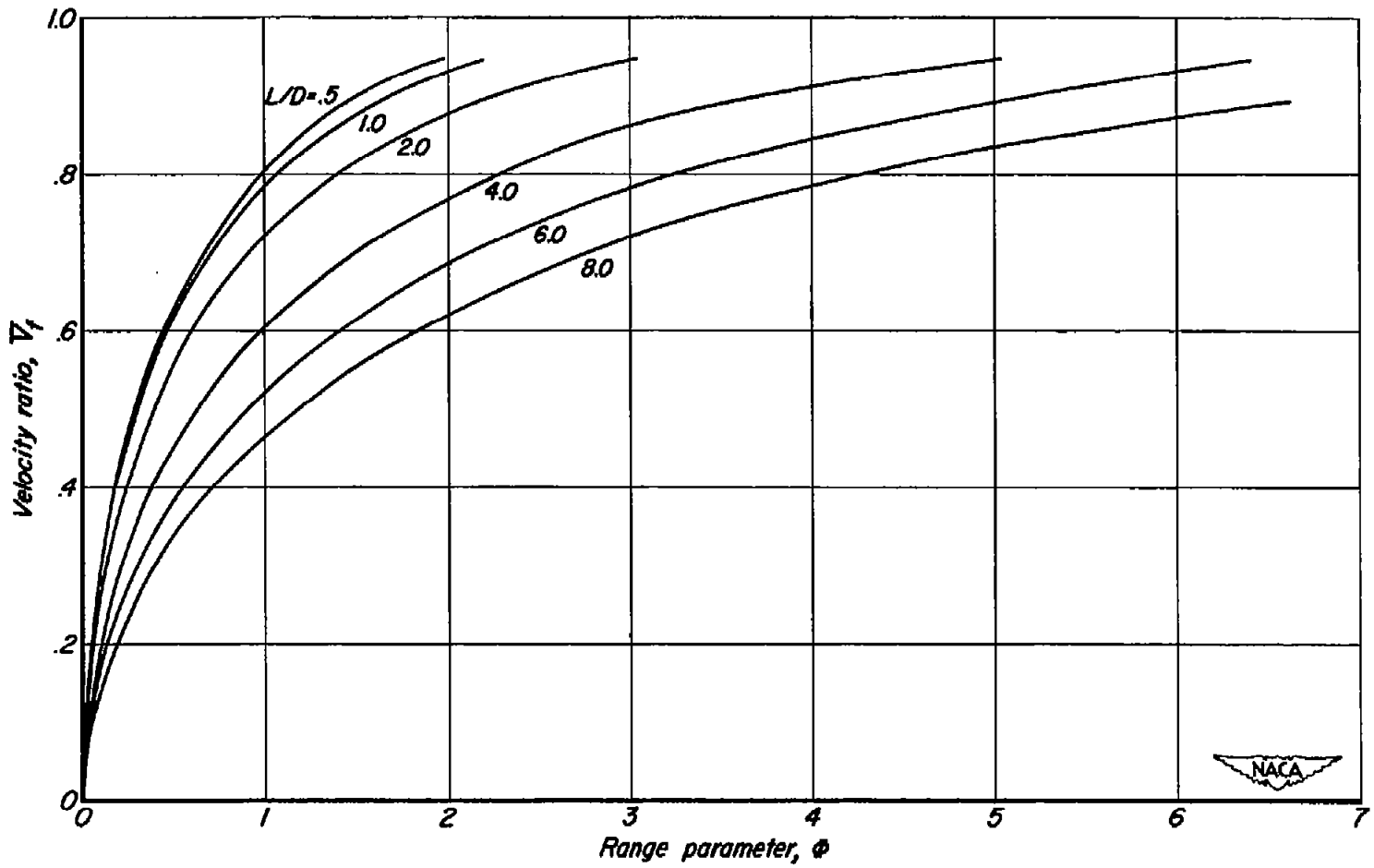


Figure 4.- Variation of velocity with range for various values of lift-drag ratio for skip vehicle.

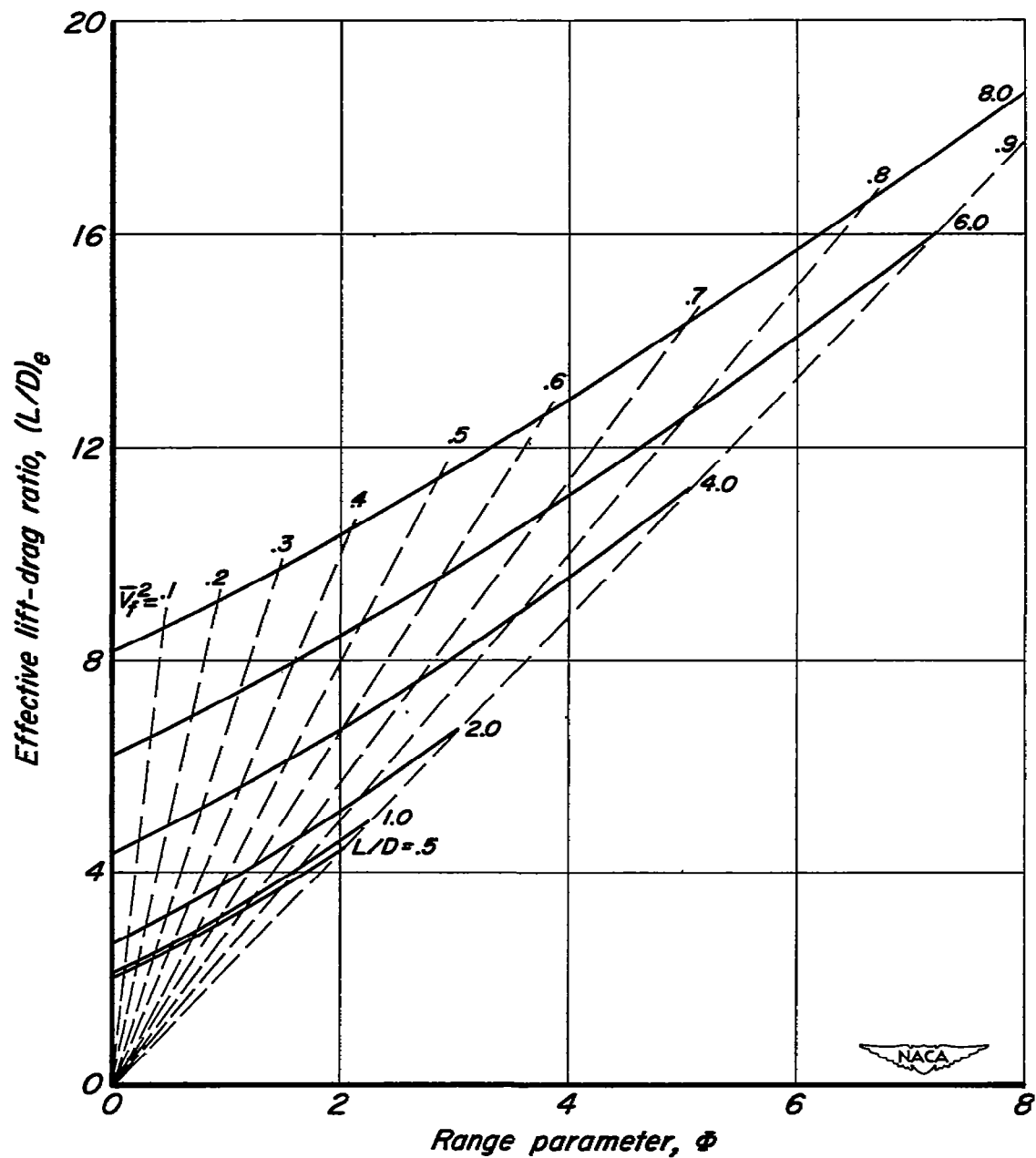


Figure 5.— Variation of effective lift-drag ratio with range for various values of aerodynamic lift-drag ratio of skip vehicle.

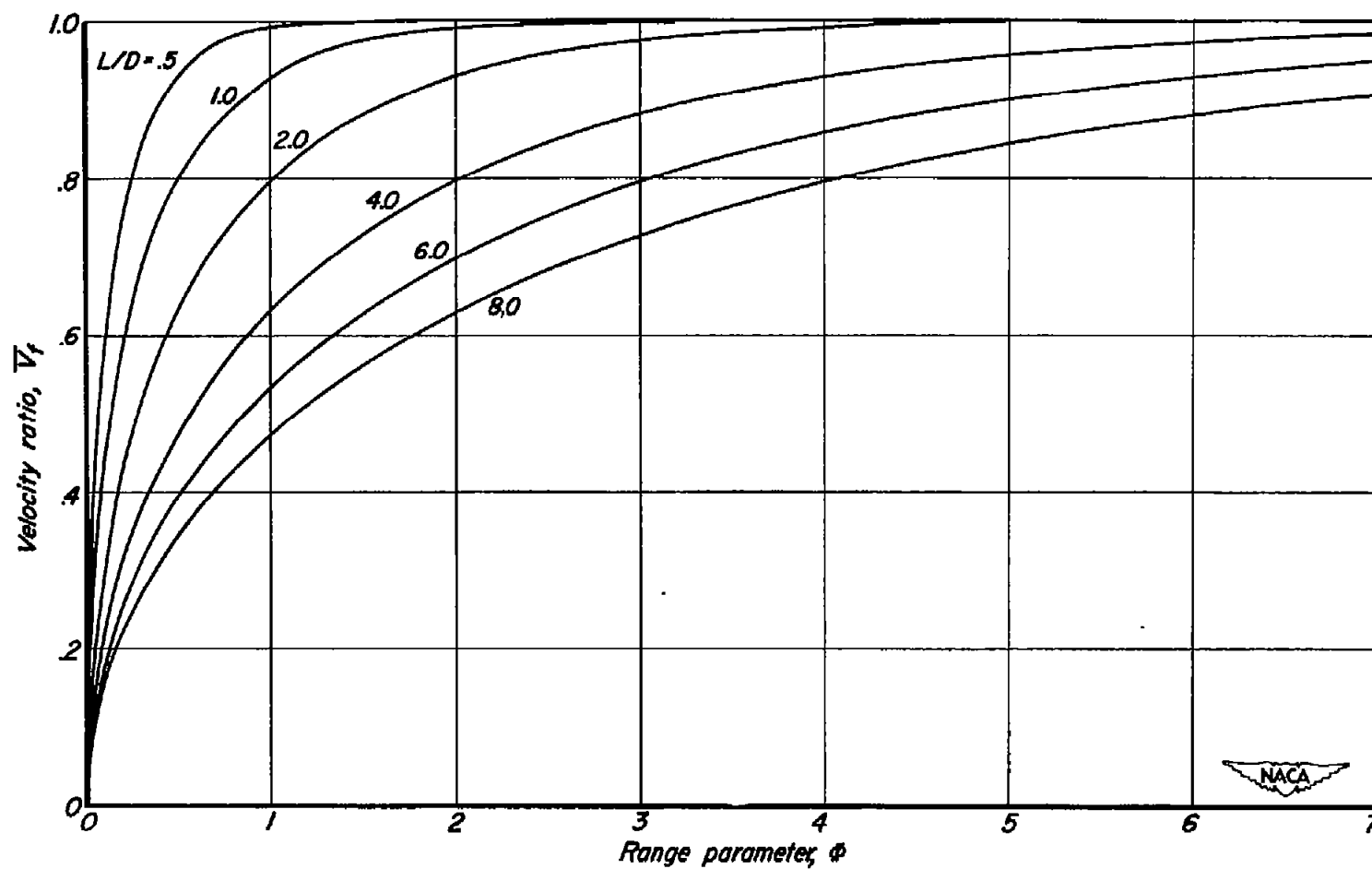


Figure 6.— Variation of velocity with range for various values of lift-drag ratio of glide vehicle.

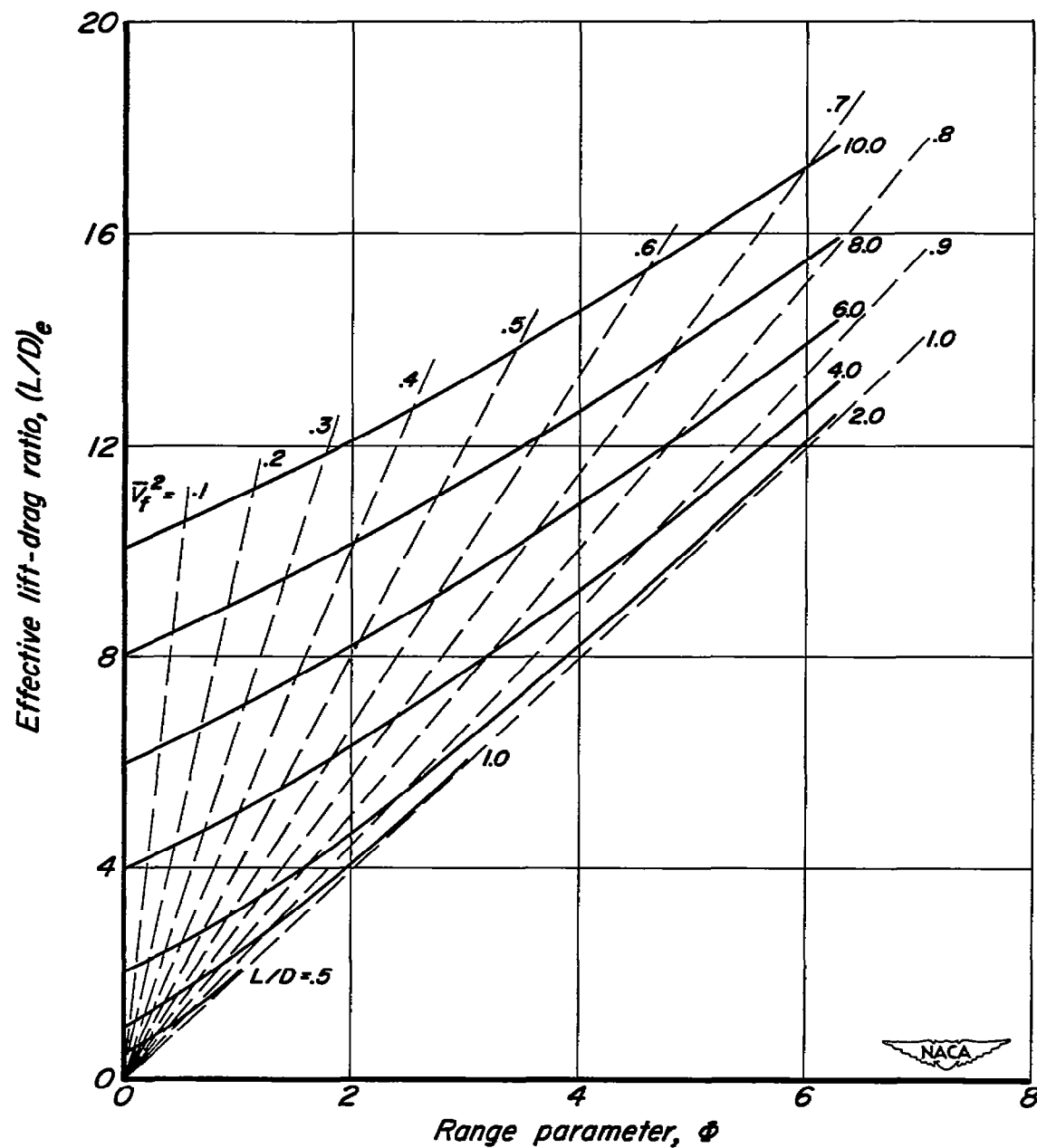


Figure 7.— Variation of effective lift-drag ratio with range for various values of aerodynamic lift-drag ratio of glide vehicle.

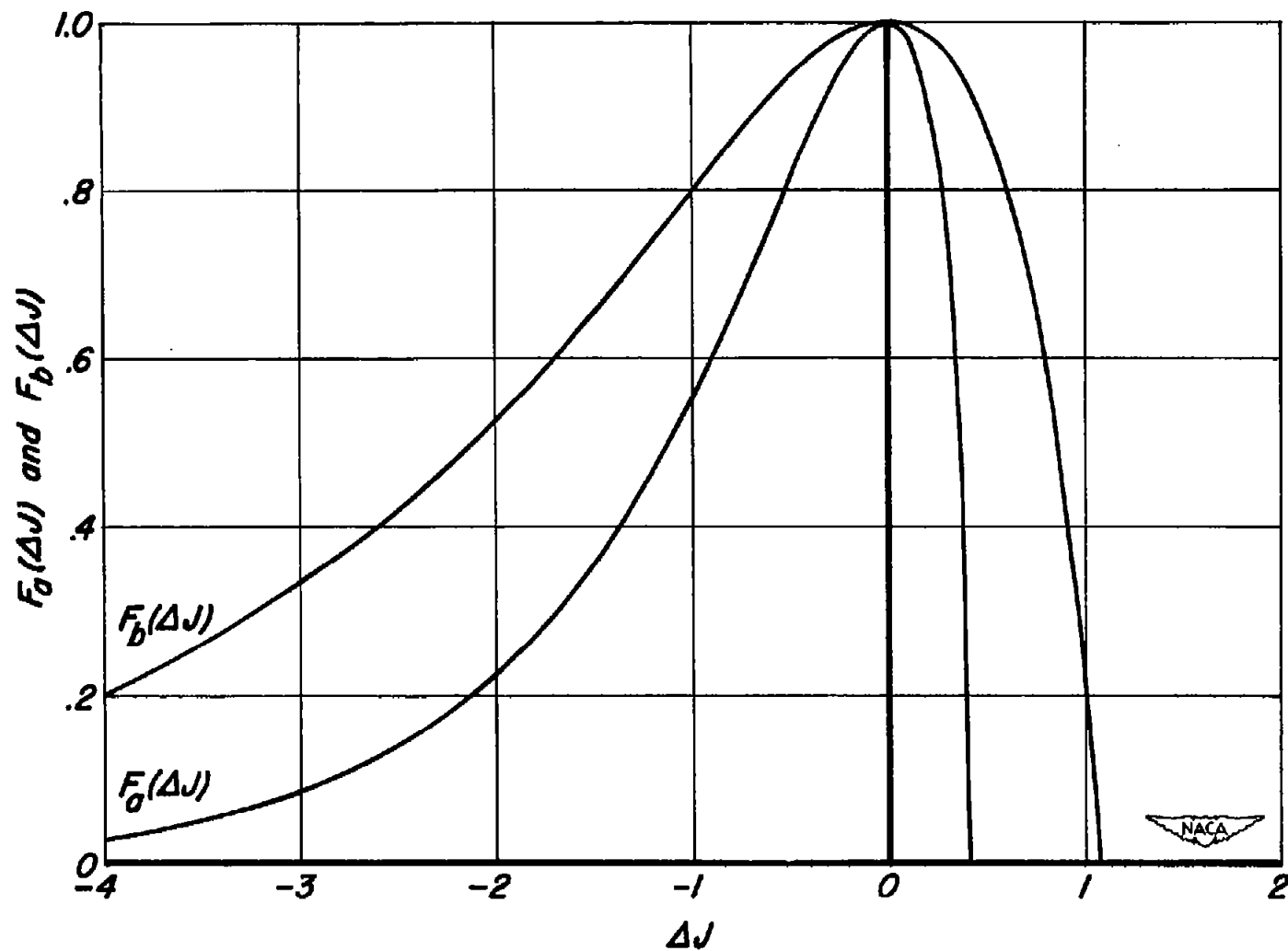


Figure 8.— Variations of $F_0(\Delta J)$ and $F_b(\Delta J)$ with ΔJ .

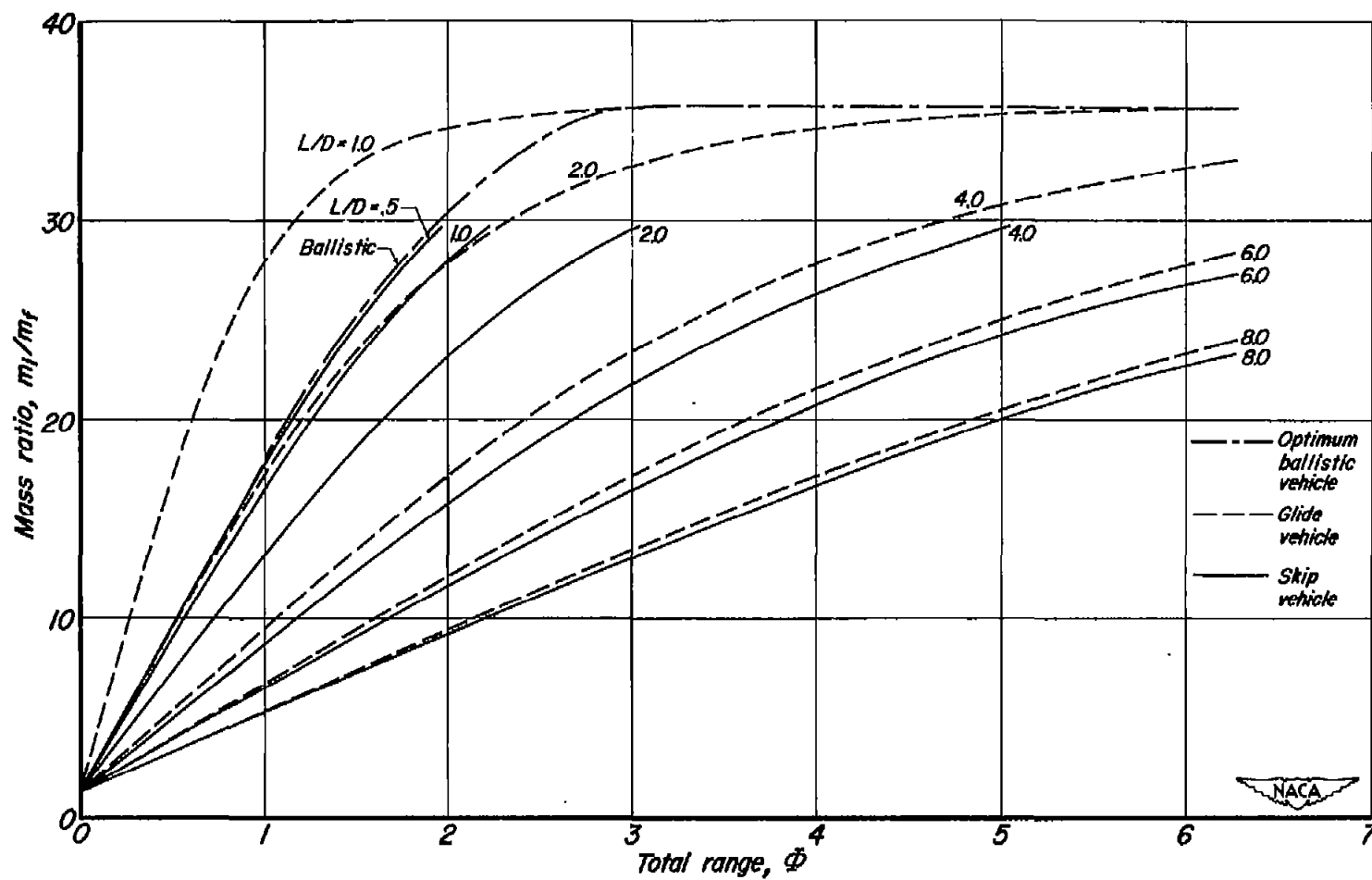


Figure 9.— Variation of mass ratio with range for various lift-drag ratios of hypervelocity vehicles.

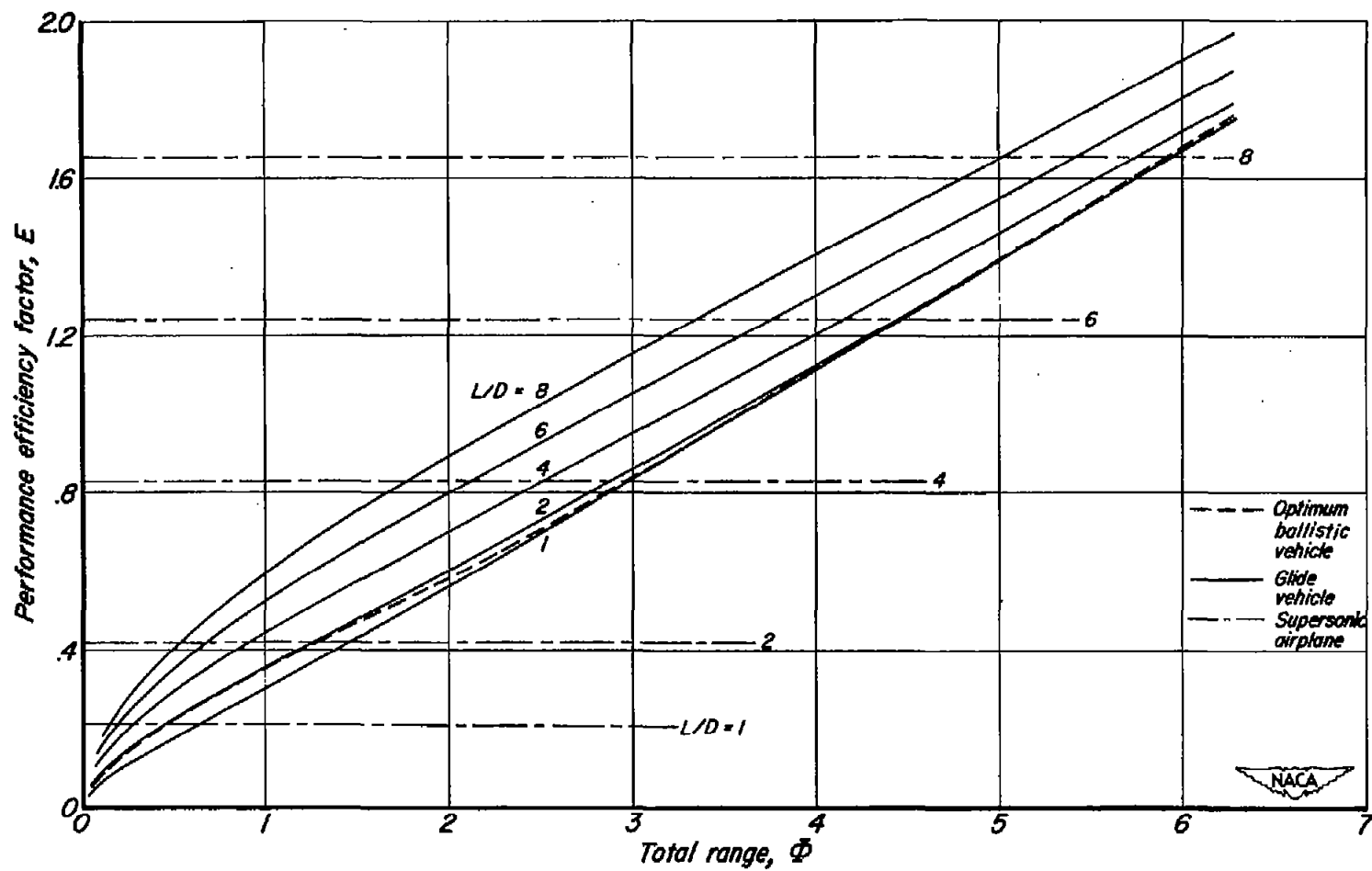


Figure 10.- Variation of performance efficiency factor with total range for ballistic and glide vehicles and the supersonic airplane.

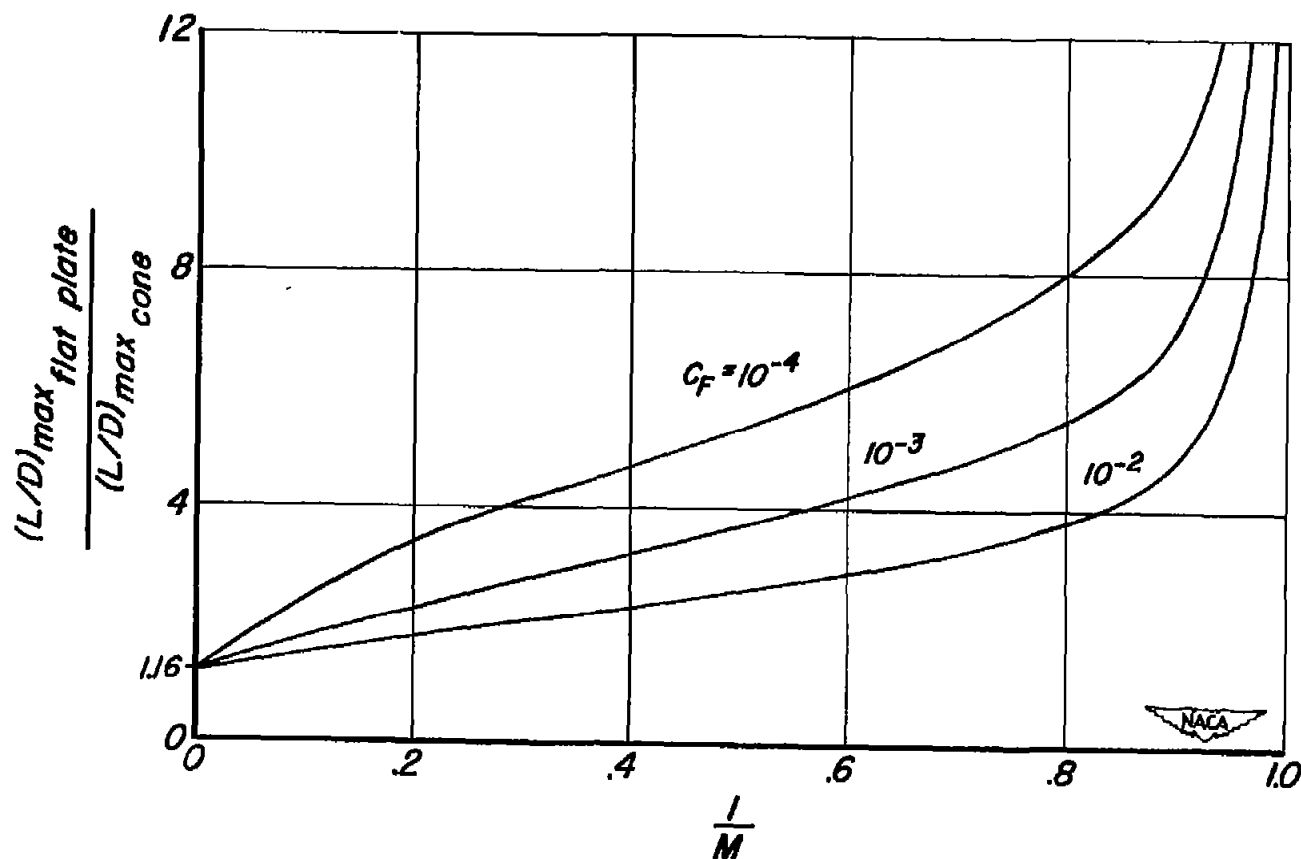


Figure 11.— Variation with reciprocal Mach number of the ratio of $(L/D)_{\max}$ of a flat plate to $(L/D)_{\max}$ of optimum cones for various values of skin-friction coefficient.

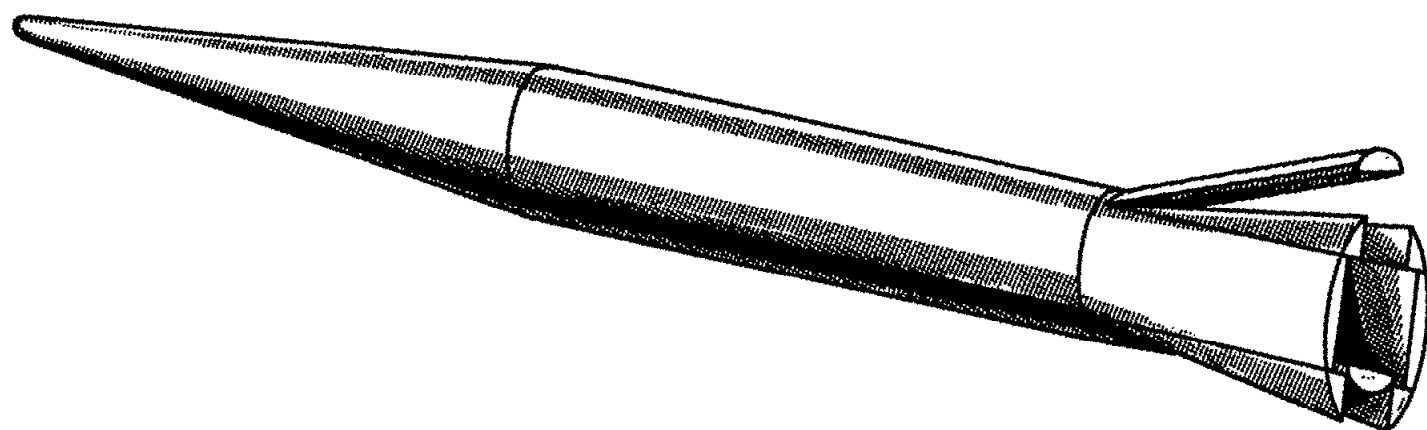


Figure 12.- Sketch of wingless glide vehicle.

NACA RM A51110

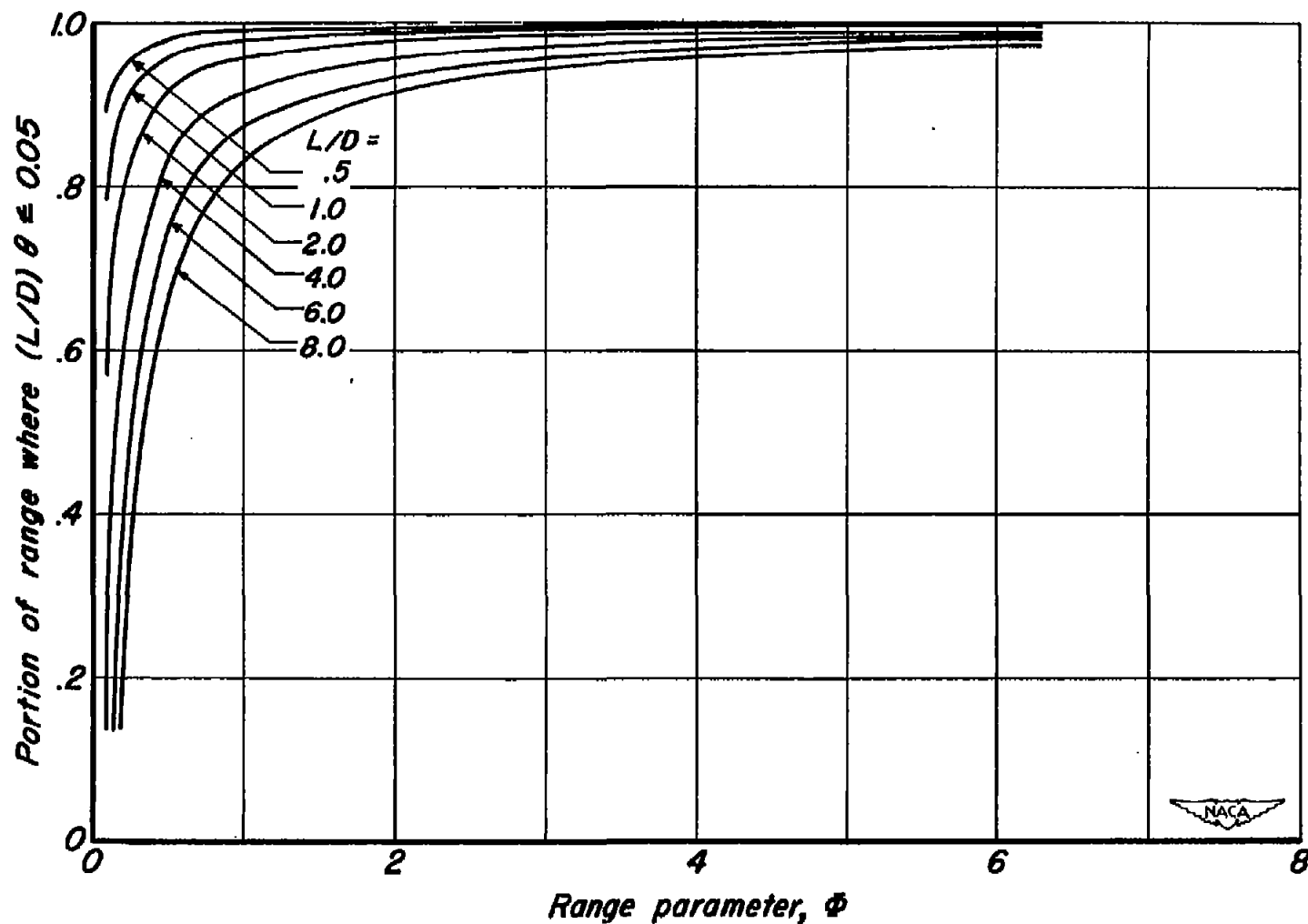


Figure 13.- Portion of range where $(L/D) \theta \leq 0.05$ as a function of range for various values of lift-drag ratio.

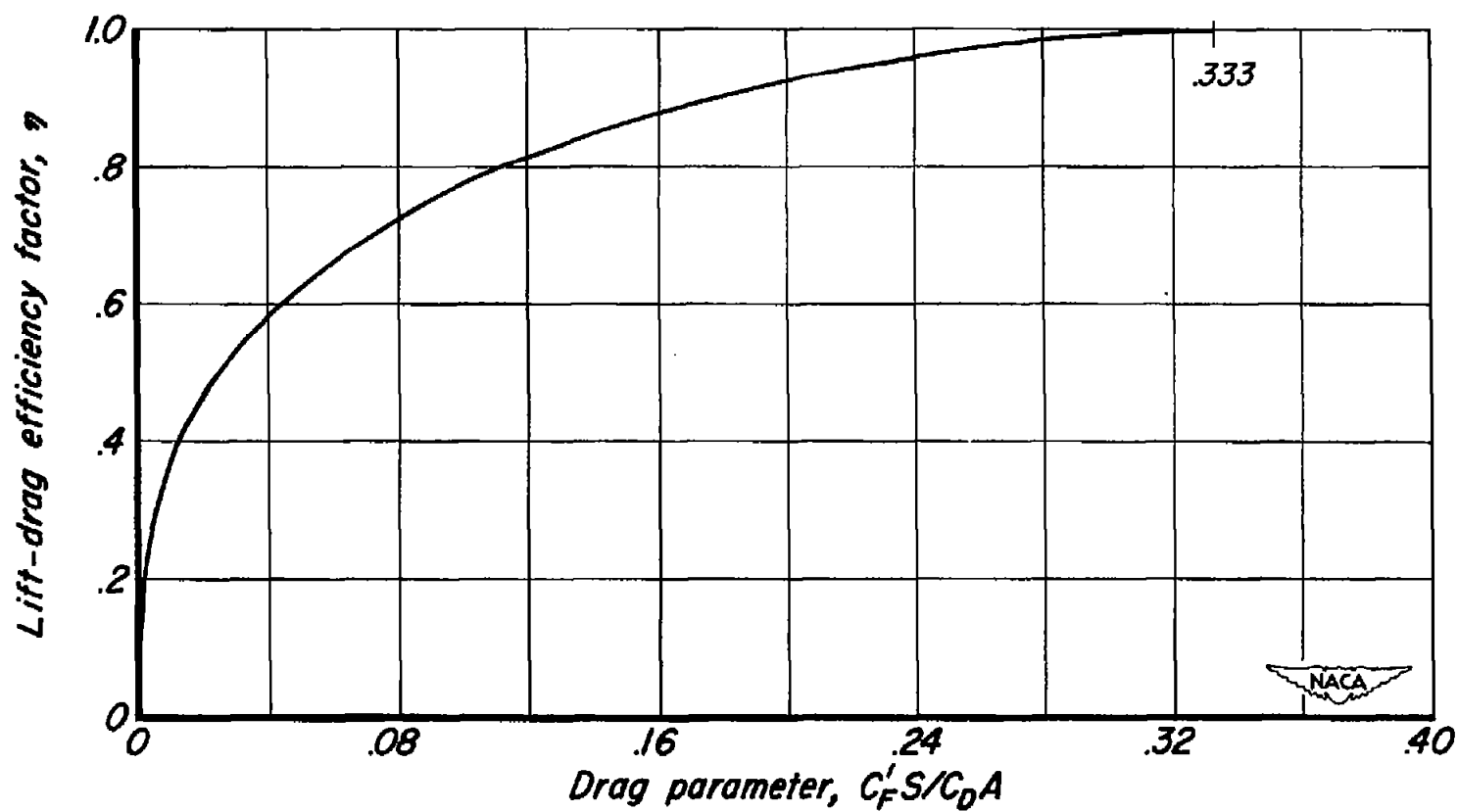


Figure 14.— Variation of lift-drag efficiency factor with drag parameter for cones.

~~CONFIDENTIAL~~



~~CONFIDENTIAL~~